N O T I C E

NASA CR-166666

SPACE SCIENCES LABORATORY

FINAL REPORT: UNIVERSITY OF CALIFORNIA ELECTRON AND X-RAY

EXPERIMENTS ON ISEE-3. CONTRACT NAS5-22307.

Kinsey A. Anderson
Principal Investigator
University of California
Berkeley, CA 94720

January 1981
Final Report for period 11 April 1975 - 31 October 1980

Prepared for

Goddard Space Flight Center
Greenbelt, MD 20771

UNIVERSITY OF CALIFORNIA, BERKELEY

1. Report No.	2. Government Accession No.	3. Recipient's Catalog No.
4. Title and Subtitle FINAL REPORT: UNIVERSITY OF CALIFORNIA ELECTRON AND X-RAY EXPERIMENTS ON ISEE-3. CONTRACT NAS5-22307		5. Report Date
		6. Performing Organization Code
7. Author(s) K. A. Anderson		8. Performing Organization Report No. series 22, issue 3
9. Performing Organization Name and Address Space Sciences Laboratory University of California Berkeley, CA 94720		10. Work Unit No.
		11. Contract or Grant No. NAS5-22307
		13. Type of Report and Period Covered
12. Sponsoring Agency Name and Address NASA Goddard Space Flight Center Greenbelt, MD		Final Report 4/11/75 - 10/31/80
		14. Sponsoring Agency Code

15. Supplementary Notes

16. Abstract

The history of the University of California Solar and Inter-
planetary Electron Experiment and the Solar X-Ray Experiment
is outlined, and descriptions of the two instruments are given.
The roles of the personnel are described and the data analysis
projects completed or begun are summarized. A bibliography
is included.

17. Key Words (Selected by Author(s)) Final Report: U.C. Berkeley ISEE-3 Experiments	18. Distribution Statement Unlimited		
19. Security Classif. (of this report) Unclassified	20. Security Classif. (of this page) Unclassified	21. No. of Pages	22. Price*

*For sale by the Clearinghouse for Federal Scientific and Technical Information, Springfield, Virginia 22151.

TABLE OF CONTENTS

FINAL REPORT: NAS5-22307

I.   INTRODUCTION

The NASA contract under which the University of California participation in
the ISEE-3 spacecraft mission was supported began on 11 April 1975 and ex-
pired 31 October 1981. During that time two separate spaceflight experiments,
each with its distinctly different set of scientific objectives, were designed,
fabricated, tested, and flight qualified. In addition, the contract NAS5-22307
supported about two years of post launch data reduction and analysis.

Scientifically, both experiments have turned out to be enormously rewarding.
Both have provided discoveries of unexpected phenomena, and many cooperative
projects were initiated during the report period.

The success of the two experiments came despite several difficulties, the
most serious of which were:

1) A failure in the project management at Berkeley which required a change
of engineering personnel at a late date in the hardware schedule.

2) The NASA Headquarters' imposition of a $1,500,000 ceiling on the build-
ing cost of the two experiments. This "take-it-or-leave-it" proposition
required taking a high-risk subcontractor who had submitted the lowest
bid. Performance by this subcontractor was less than satisfactory, and
the failure of one of the experiments about 15 months after launch can
doubtlessly be traced to difficulties resulting from the arbitrarily
restricted budget and the poor subcontractor performance.

We can report, however, that at the end of the contract period, both instru-
ments were performing well and providing data of high quality. A detailed veri-
fication of expected instrument performance came soon after launch by means of
a "Black Box" installed at GSFC. The "Black Box" stripped off the telemetry
words for the two UCB-Space Sciences Laboratory experiments and put them on a

telephone line. The words were received at Berkeley and processed, then dis-
played in several ways. By this means we could see that the instruments were
working and that all modes of operation could be exercised. The backgrounds
were determined, and the effects of quiet-time x-ray emission from the sun were
evaluated.

II. DESCRIPTION OF THE SOLAR AND INTERPLANETARY ELECTRON EXPERIMENT

III. DESCRIPTION OF THE SOLAR X-RAY EXPERIMENT

A. The X-Ray Spectrometer Experiment

B. Description of the Electronics

C. In-Flight Testing and Calibration

During the period of time between the launch of ISEE-C and the present, the AN-04 x-ray instrument has undergone several thorough self-test programs. These tests are always coordinated with command sequences sent by ISEE control at MSOCC and the remote operation of the SSL "Black Box" communications processor at MSOCC which links the NASCOM data line to the SSL Datalab computer. In this way, the instrument performance during self-test, and at other times, is monitored in real-time at Berkeley for immediate evaluation and correction.

The primary built-in self test circuits consist of a digital test pulse generator (TP6) and an analog TP6. When commanded on, the digital TP6 generates a series of pulses designed to test all of the floating point accumulators at various breakpoints and simulates solar flare and gamma burst conditions to test interface logic between the x-ray instrument and the Los Alamos memory unit, and also logic within the memory. The analog TP6 inserts a sequence of shaped

pulses at the detector outputs to test the overall throughput of the instrument but primarily the health of the front-end electronics and the pulse height analyzers.

Additional tests consist of enabling automatic gain control (AGC) loops on each detector to allow the detector's gain to be served to a built-in radioactive calibration source. This permits measurement of possible changes in the detector gain. The response of the AGC loop to commanded offsets also yields a measure of the energy resolution of each detector. The latest tests to date were performed on January 20, 1981; results indicate that the instrument continues to perform satisfactorily with no electronic malfunctions and only a relatively small aging of the detectors.

IV.   DATA PROCESSING AND ANALYSIS

A.   Solar and Interplanetary Electron Experiment

A large number of investigations were begun under NAS5-22307.   Following are summaries of these investigations.

1)   Dr. Robert P. Lin.   I have analyzed the production of plasma waves and the generation of type III solar radio emission using our ISEE-3 measurements of the electron distribution function. This work was done in collaboration with D. A. Gurnett (U. Iowa) and F. L. Scarf (TRW).   A second collaboration with G. de Genouillac and J. L. Steinberg (Meudon) was primarily concerned with the radio emission/energetic electron characteristics.

   I have systematically studied the background quiet-time electron population from 2-200 keV, with the assistance of Robert Campbell.   S. R. Kane, Nicole Vilmer (Meudon) and I studied the hard x-ray/electron relationship in flares, particularly the spectral characteristics.   I have also looked at the spectral characteristics of solar flare impulsive particle events, particularly at low energies, where only very few measurements have been obtained before.

2)   Mr. Douglas W. Potter.   I spent most of the year after the ISEE-3 launch working on the data analysis programs.   The sections on Instrumentation and Data Analysis contained in Appendix A of this report are drafts of parts of my Ph.D. dissertation.   I have also worked on low energy impulsive solar electron events.   (See Appendix D for one paper on this subject.)   I have been working on electron acceleration at interplanetary shocks.   Although electron acceleration has rarely been observed, I find that it is a common feature at the relatively low energies that we measure.

3) <u>Dr. K. A. Anderson</u>. Two data analysis projects were begun during the reporting period:

a) <u>Measurements of Bow Shock Particles Far Upstream from Earth</u>. The ability of the particle experiment to make highly resolved pitch angular distributions has opened the door for a renewed attack on this long standing problem. The experiment also provides energy spectra of the bow shock electrons in an energy range where they have not been measured before--2 to 10 keV. Results from these topics were presented at the Upstream Particle Workshop at JPL in April 1980, and the writing of an article was begun in the summer of 1980.

b) <u>Measurements of Low Energy Electrons and Ions during Long-Lived Solar Particle Events</u>. An abstract of this paper, which was written with R. P. Lin and D. W. Potter, follows:

Following a solar flare in April 1979, a stream of ions and electrons appeared in interplanetary space for about 8 days. The ions follow a classic ESP pattern. Large fluxes of low energy (2 - 11 keV) electrons are also present throughout the event. Several distinct populations of these electrons can be identified in association with filaments of interplanetary magnetic field. The electron energy spectrum is remarkably well fit by a power law exponent -2.7 during most of the event.

The pitch angle distribution of the low energy electrons are complex and undergo many changes. Weak pitch angle scattering and adiabatic effects play a role in shaping these distributions. The low energy electron fluxes increase following the strong interplanetary shock on 5 April 1979.

This work was presented in an invited paper at the Study of Travelling Interplanetary Phenomena Workshop held in Smolenice, Czechoslovakia during June 1980 and will be published in the Workshop Proceedings.

B. Solar X-Ray Experiment

The ISEE-3 x-ray experiment is providing valuable new data related to two astrophysical phenomena, viz. solar flares and cosmic gamma-ray bursts. The solar flare data are processed and analyzed at Berkeley. The data related to cosmic gamma-ray bursts are analyzed primarily at the Los Alamos Scientific Laboratory. Here we will be concerned only with the data processing and analysis performed at Berkeley.

Data Analysis Projects

A number of solar x-ray studies were begun during the reporting period. They involve collaborations with astrophysicists at other institutions in the U.S., as well as in other countries such as France, Japan and Switzerland. The projects can be broadly divided into three groups:

1) Projects which involve similar x-ray detectors aboard other space-craft such as Pioneer Venus Orbiter (PVO), Venera 11-12 and Helios-2, which provide a stereoscopic view of the solar flares and also high time resolution measurements of solar x-ray emissions. These studies involve collaboration with the following institutions:

    Los Alamos Scientific Laboratory

    University of Toulouse, France

    Goddard Space Flight Center

2) Projects which involve simultaneous observations of solar flares at radio and optical wavelengths made with ground-based radio and optical telescopes. These studies involve collaboration with the following institutions:

    Observatoire de Paris, France

    Tokyo Astronomical Observatory, Japan

    Radio Astronomy Group, Zurich, Switzerland

    U.S. Air Force Geophysics Laboratory, Massachusetts

California Institute of Technology

3) Projects which involve participation in International Programs de-
signed for a well coordinated study of solar flares observed with
space-borne as well as ground-based instruments operated by a
large number of countries. One such program is the Solar Maxi-
mum Year (SMY), which consists of the following three projects:

   Flare Build-up Study (FBS)

   Study of Energy Release in Flares (SERF)

   Study of Travelling Interplanetary Phenomena (STIP)

The ISEE-3 x-ray data plays a central role in the collaborative projects
(1) and (2) and provides valuable information for project (3).

Data Processing Plan

Two types of computers are available for the x-ray data processing at
Berkeley: the large CDC 7600 at the Lawrence Berkeley Laboratory (LBL) and the
mini-computers Interdata 70 and 732 at the Space Sciences Laboratory (SSL).
There are different advantages in using the different computers for the x-ray
data processing. While the LBL computer has a large memory, microfiche facili-
ties and relatively small data handling requirements, the SSL computers have
interactive capabilities. Hence the basic data processing is primarily done on
the LBL computer. The SSL computer is mostly used for further analysis of the
data.

Figure 1 (page 9) shows the x-ray data processing plan. Each GSFC data
tape that is sent contains a week's worth of data. It has both the XRAY and
PARTICLE experiment data. The first part of the processing consists of making
passes through the tape and creating two edit tapes, one for XRAY and one for
PARTICLE. This process is performed on the INTERDATA 70 with the program ICRUN2.
It rearranges the data into one day per file and eliminates data overlaps between
files and bad records. Program ICDMPO gives a formatted point by point dump of
the original tape. It also runs on INTERDATA 70. Program ICDMP generates a

Figure 1

ISEE-3 X-RAY DATA PROCESSING PLAN
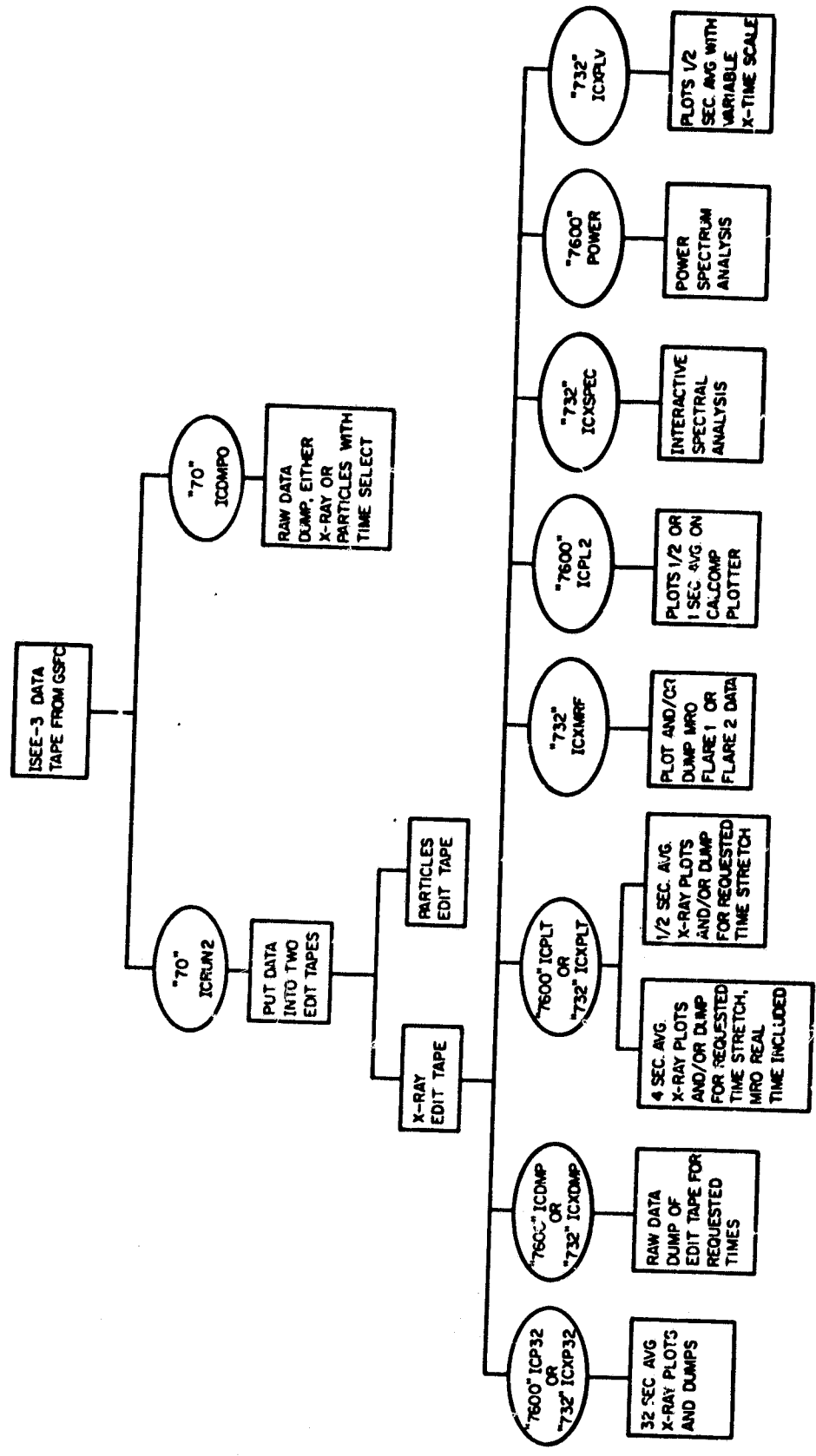
the original tape. It also runs on INTERDATA 70. Program ICDMP generates a formatted point by point dump of the edit tape, with no conversion to the data.

Programs are also available to display the x-ray data in various ways. Program ICP32 generates 32 second average plots and listings. This provides a quick scan through all the available data, and interesting data are selected for more detailed displays. For the selected data, program ICPLT generates 4 second or 1/2 second average plots and listings. If 4 second averages are chosen, the MRO real time data are included in the plots and dumps for particular plot sets. For the x-ray data which are in MRO stored mode, program ICXMRF, which runs on the 732, generates point by point plots in linear or logarithmic scale and also provides point by point dump of available channels. Once all the selected data are analyzed, bursts are selected for spectral analysis. This requires some interactive abilities and is done on the INTERDATA 732.

The basic "production" type processing has been completed for the x-ray data obtained from launch in August 1978 through November 1980. Since the x-ray experiment is still performing satisfactorily, this data processing will continue as new data tapes become available from GSFC.

The processing and analysis of the data are the primary responsibilities of the programmer and project scientist, respectively. The basic data processing is carried out with the help of undergraduate students employed as engineering aids. Under the supervision of the programmer, these aids submit "jobs" to the LBL and SSL computers and help in cataloging and filing the processed data. Under the supervision of the project scientist, the aids also perform other tasks such as minor computations and graphing relevant to the analysis of the processed data.

V. BIBLIOGRAPHIES

A. Solar and Interplanetary Electron Experiment

1. An experiment to measure interplanetary and solar electrons, K. A. Anderson, R. P. Lin, D. W. Potter, and H. D. Heetderks, IEEE Trans. Geosc. Elec., GE-16, No. 3, 153-156, 1978.

2. Observations of suprathermal particles in the interplanetary medium, R. P. Lin, in press, Solar Wind, 4, ed. H. Rosenbauer, Springer, N.Y.-Heidelberg-Berlin, 1979.

3. Energetic particles in space, R. P. Lin, Solar Physics, 67, 393, 1980.

4. Impulsive 2-10 keV solar electron events not associated with flares, R. P. Lin, D. W. Potter and K. A. Anderson, Ap. J., 236, L97, 1980.

5. Distribution functions of type III electrons observed in interplanetary space, R. P. Lin, D. W. Potter, J. Fainberg, R. G. Stone, and J. L. Steinberg, Radiophysics of the Sun, ed. M. R. Kundu and T. E. Gergely, 311, 1980.

6. Measurement of low energy electrons and ions during long-lived solar particle events, K. A. Anderson, R. P. Lin and D. W. Potter, to be published in Travelling Interplanetary Phenomena: Shock Waves in the solar Corona and Interplanetary Space, Reidel Publishing Co., 1981.

7. Measurements of bow shock particles far upstream from earth, K. A. Anderson, submitted for publication to J. Geophys. Res., September, 1930.

8. Propagation of low energy solar electrons, K. A. Anderson, J. P. McFadden and R. P. Lin, submitted for publication, Geophys. Res. Lett., 1981.

9. Energetic electrons and plasma waves associated with a solar type III radio burst, R. P. Lin, D. W. Potter, D. A. Gurnett, and F. L. Scarf, to be submitted to Ap. J.

10. Characteristics of the electron beam in type III radio bursts, G. de Genouillac, R. P. Lin, and J. L. Steinberg (in preparation).

B. Solar X-Ray Experiment

1. X-ray spectrometer experiment aboard the ISEE-C (Heliocentric) spacecraft, K. A. Anderson, S. R. Kane, J. H. Primbsch, R. H. Weitzmann, W. D. Evans, R. W. Klebesadel, and W. P. Aiello, IEEE Trans. Geosc. Elec., GE-16, No. 3, 157-159, 1978.

2. Observation of an impulsive solar x-ray burst from a coronal source, S. R. Kane, K. A. Anderson, W. D. Evans, R. W. Klebesadel, and J. Laros, Ap. J. Lett., 233, L151, 1979.

3. Directivity of 50-100 keV x-ray emission from impulsive solar flares, S. R. Kane, K. A. Anderson, W. D. Evans, R. W. Klebesadel, and J. Laros, Ap. J. Lett., 239, L85, 1980.

4. Correlated observations of a spatially resolved type III solar radio burst group and the associated hard x-ray emission, S. R. Kane, M. Pick and A. Raoult, Ap. J. Lett., 241, L113, 1980.

5. Multi-spacecraft observations of solar hard x-ray bursts, S. R. Kane, Astrophys. & Space Sc., in press, 1980.

6. On the relationship between soft x-rays and Hα emitting structures during a solar flare, H. Zirin, U. Feldman, G. A. Doschek and S. R. Kane, Solar Phys., in press, 1981.

7. Recent observations of energetic electrons in solar flares, S. R. Kane, Solar and Interplanetary Dynamics, eds. M. Dryer and E. N. Tandberg-Hanssen, D. Reidel Publ. Co., 227, 1980.

8. Observation of a coronal impulsive x-ray burst and its implications regarding the associated microwave source, S. R. Kane, Radio Physics of the Sun, eds. M. R. Kundu and T. E. Gergely, D. Reidel Publ. Co., 443, 1980.

9. X-ray burst observations from the UCB/LASL experiment on ISEE-3, W. D. Evans, R. W. Klebesadel, J. G. Laros, J. Terrell and S. R. Kane, Nature, 286, 784.

10. Radial motion of electron acceleration region during a solar flare, S. R. Kane and A. Raoult, to be submitted to Ap. J. Lett.

11. Characteristics of the hard x-ray and metric-decimetric radio sources in 4 Dec. 1978 solar flare, S. R. Kane and R. Treumann, to be submitted to Solar Phys.

12. Hard x-ray and microwave source characteristics in a large solar flare, S. R. Kane, H. S. Sawant and N. Vilmer, to be submitted to Ap. J.

13. Large amplitude oscillations of hard x-ray and microwave emissions in 7 June 1980 solar flare, S. R. Kane, K. Kai and S. Enowe, to be submitted to Ap. J. Lett.

14. Meter-decimeter bursts and the associated hard x-ray emission, M. R. Kundu, T. E. Gergely and S. R. Kane, to be submitted to Solar Phys.

VI. ABSTRACTS OF TALKS BASED ON ISEE-3 RESULTS

PARTICLE MEASUREMENTS NEAR THE FRONT OF INTERPLANETARY SHOCK WAVES

D.W. Potter
K.A. Anderson (both at: Space Sciences
   Laboratory and Physics Department, University
   of California, Berkeley, CA 94720)
R.P. Lin (Space Sciences Laboratory, University
   of California, Berkeley, CA 94720)

We have examined the particle effects at the front of several interplanetary shock waves using the University of California particles instrument on ISEE-3. As the shock wave passes, the electron flux increases over a wide energy range of two keV up to a few hundred keV. An increase in the proton flux above 50 keV also occurs.

The shock waves seem to fall into two categories: 1) The electron flux increases in a step-like fashion. The step occurs on a time scale of less that two minutes. The shock is likely to be quasi-perpendicular. 2) The electron flux fluctuates over a period of ten to forty minutes as it increases to a new level. The shock is likely to be quasi-parallel.

At two keV, the electrons are aligned with the magnetic field. Often there are relatively no particles at pitch angles in the vicinity of 90°. As the shock passes, the anisotropy of the electrons either stays constant or increases slightly.

1. Fall Meeting, 1979

2. 045457 POTTER

3. Douglas W. Potter
   Space Sciences Laboratory
   University of California
   Berkeley, CA 94720

4. SS (Solar and Interplanetary Physics)

5.

6. Oral

7. 0%

8. a. Accounting Office
   b. 2-26332
   c. Student Rate

9. C

OBSERVATIONS OF SOLAR ELECTRON EVENTS BELOW 10 keV

D. W. Potter
R. P. Lin
K. A. Anderson (all at: Space Sciences Laboratory, University of California, Berkeley, California 94720)

The University of California particles experiment on ISEE-3 observed six small impulsive solar electron events during 4-8 November 1978. These events are unusual in that they are observed primarily at energies below $\sim$ 10 keV, with several events showing no flux increase above 20 keV. The energy spectra for these events is well approximated by a power law with no appreciable fall-off at energies down to 2 keV. Thus the electrons appear to be accelerated high in the solar corona. The close grouping in time suggests that these events are associated with a single active region.

The angular distributions are sharply peaked around the magnetic field line. The distributions become less anisotropic with increasing energy. Maximum to minimum ratios range from greater than 50:1 at 2 keV to 4:1 at 20 keV. The minimum in the angular distribution oftentimes occurs at right angles to the field line.

1. 04547

2. 1979 Spring Meeting

3. SPR

4. None

5. No

6. No

7. None

8. Accounting Office
    Space Sciences Laboratory
    University of California
    Berkeley, CA 94720

9. 26332

EVIDENCE FOR H⁻ IONS IN THE SOLAR WIND

K.A. Anderson, R.D. Campbell, R.P. Lin, and D.W. Potter (all at: Space Sciences Laboratory, University of California, Berkeley, California 94720)

Observations from the large area electron electrostatic analyzer of the U.C. Berkeley energetic particle experiment on ISEE-3 show the occasional presence of particles flowing in the anti-solar direction, i.e., the flow direction of the solar wind. These particles are only observed in the lowest three energy charge channels centered at 2.0, 2.33 and 2.66 keV/q, and only in the Sun sector and sometimes one adjacent sector, out of 16 sectors. The occasions when these particles are observed are times of enhanced solar wind velocity. The observations are consistent with H⁻ ions flowing with the solar wind. We have made laboratory measurements of the response of the electrostatic analyzer to positive ions. These measurements indicate that contamination by postively charged solar wind ions is unlikely to be responsible for the observations. We will discuss possible sources for H⁻ ions in the solar wind.

1. 1978 Fall American Geophysical Meeting.

2. Solar and Interplanetary Physics, Solar Wind 1.

3. Oral only.

DISTRIBUTION FUNCTIONS OF TYPE III ELECTRONS OBSERVED IN INTERPLANETARY SPACE

R.P. Lin, D.W. Potter, K.A. Anderson (all at: Space Sciences Laboratory, University of California, Berkeley, CA 94720)

J. Fainberg, R.G. Stone (both at: Goddard Space Flight Center, Greenbelt, MD 20771)

J.L. Steinberg (Department de Recherches Spatiales, Observatoire Meudon, 92190 Meudon, France)

1. Fall Meeting, 1979

2. 002588 LIN

3. R. P. Lin
   Space Sciences Laboratory
   University of California
   Berkeley, CA 94720

4. SS

5. Basic Plasma Processes
   in Space

6. 0

7. 10, I.A.U.

8. Accounting Office
   Space Sciences Laboratory
   University of California
   Berkeley, CA 94720

9. C

We present simultaneous energetic electron and solar radio observations from the ISEE-3 spacecraft of several solar type III radio bursts. The UC Berkeley energetic particle experiment measures from 2 to $\sim 10^3$ keV with good energy and pitch angle resolution while the Meudon/GSFC radio experiment tracks type III radio bursts at 24 frequencies in the range 30 kHz - 2 MHz.

Two types of electron events are observed by the particle experiment: (1) the "normal" type of 20 to > 100 keV flare associated electron events reported previously, and (2) events where only electrons in the 2-10 keV range are observed. These low energy events are not associated with flares or high frequency (> 10 MHz) radio emission but rather they appear to be associated with individual type III bursts from low frequency type III storms. Both types of electron event are closely correlated to the very low frequency type III emission produced in situ at 1 A.U.

We have made preliminary computations of the electron velocity distribution function parallel to the magnetic field, $f(v_{\parallel})$, for several events. In the > 20 keV events no strong positive slope $\dfrac{df(v_{\parallel})}{dv} > 0$ is observed, rather $f(v)$ has a plateau-like shape, event though a peak is observed in the energy spectra. However in the low energy electron events a peak is observed in the parallel velocity distribution function with $\dfrac{df(v_{\parallel})}{dv} > 0$ since the pitch angle distribution is very narrow, FWHM $\lesssim 22.5°$, and beamlike. For the single event where solar wind plasma density measurements were available the frequency of the radio emission is consistent with the emission being generated at the second harmonic of the plasma frequency.

LOW ENERGY ELECTRONS AND IONS IN SOLAR
PARTICLE STREAMS

K.A. Anderson
D.W. Potter
R.P. Lin (all at: Space Sciences Laboratory,
University of California, Berkeley, CA 94720)

At least sixteen solar particle streams typi-
cally lasting a few days occurred in the
September 1978 - May 1979 period for which we
have analyzed low energy electron and ion data
from the ISEE-3 spacecraft. Our instrument
measures electron energy spectra and angular
distributions from 2 keV up to several hundred
keV. In the case of protons the energy range
is 20 keV to several MeV. We find that low
energy electrons are usually fit very well by
a single power law in the range 2 to 10 keV.
There is no suggestion of turnover down to the
lowest energy. A spectrum on 4 April 1979 at
1000 UT is given by $(8 \times 10^5) E^{-2.9}$ electrons
$(sec-cm^2-ster-keV)^{-1}$ from 2 to 10 keV. At this
time the total flux is about 100 times the typ-
ical quiet time background. The electron angu-
lar distributions show remarkable variations.
Frequently they are smoothly varying with one-
dimensional anisotropies of 0.05 to 0.20.
Often, however, the flux nearly disappears
in a narrow angular interval about $\alpha = 90^\circ$ and
270°. At these times the one-dimensional ani-
sotropy varies from 0.1 to 0.5. This kind of
distribution implies very little pitch angle
scattering combined perhaps with magnetic
mirroring.

1. Fall Meeting, 1979

2. 004209 ANDERSON

3. K.A. Anderson
   Space Sciences Laboratory
   University of California
   Berkeley, CA 94720

4. SC or SS

5.

6. None

7. 0

8. Accounting Office
   Space Sciences Laboratory
   University of California
   Berkeley, CA 94720

9. C

PROPAGATION OF 2-200 keV ELECTRONS IN THE INTERPLANETARY MEDIUM

Douglas W. Potter
Kinsey A. Anderson
R.P. Lin (All from the Space Sciences
   Laboratory, University of California,
   Berkeley, CA 94720).

The high angular and energy resolution of the particles instrument on the ISEE-3 spacecraft enable us to survey the propagation character- istics of 2-200 keV interplanetary electrons under varying conditions.

We have discovered a large number of impul- sive electron events that are limited in energy to <20 keV. The extreme collimation of the particles along the field line and the shape of the flux pulse indicate that the electrons travel through the interplanetary medium with little scattering.

During long-lived solar events, quite intri- cate angular distributions are often observed. The long delay (several hours) between changes in the outward and inward going populations suggests that electrons often travel large distances (several astronomical units) from the earth before returning.

Angular distributions taken during inter- planetary shocks show that pitch angle distributions often have maximums at both zerio and 90°. Both the pre- and post-shock distributions show a maximum at zero. This indicates acceleration perpendicular to the field.

VII. APPENDICES

APPENDIX A

Description of the Solar and Interplanetary Electron Experiment

I

Instrumentation

I-A. ISEE-3 Spacecraft

The ISEE-3 (International Sun Earth Explorer) spacecraft is ideally suited for making measurements of solar particles without interference from the Earth. Launched 12 August
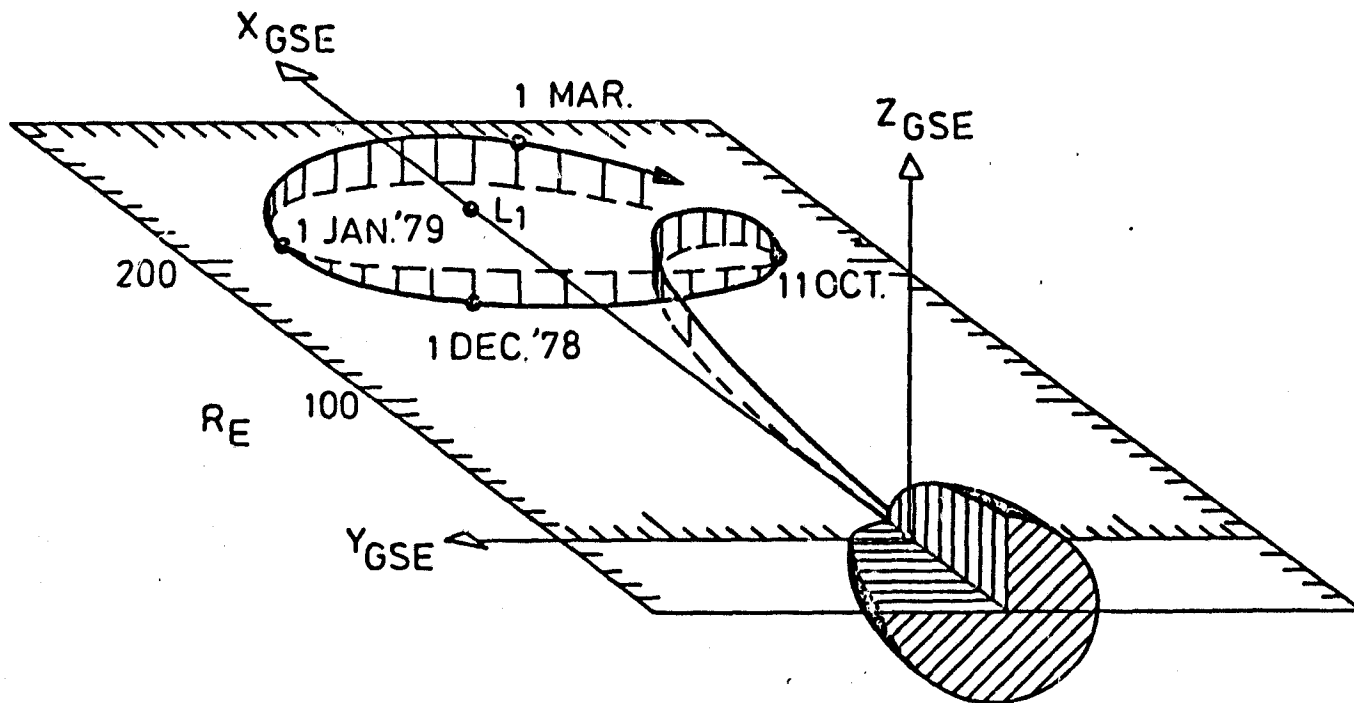
Figure I-1. ISEE-3 orbit and injection

1978, its unique orbit about the libration point (Figure I-1) on the Earth-Sun line (L_1, 230 earth radii from the Earth) places it continuously in the interplanetary medium. The spacecraft

spins once every 3 seconds about an axis perpendicular to the ecliptic.

The University of California energetic particles instrument was designed to measure elec-

Assembly	Detector	Description
ESA	E_1	Five spiraltrons
	E_p	PM tube (anticoincidence)
Foil Telescope	F_1	200 μm surface barrier detector
	F_p	PM tube (anticoincidence)
Open Telescope	O_1	200 μm surface barrier detector
	O_2	400 μm surface barrier detector
	O_p	PM tube (anticoincidence)

Table I-1. Summary of Detector Assemblies.

trons from 2 - 1000 keV and ions from 50 keV - 40 MeV with high sensitivity. As Table I-1

shows, it consists of an electrostatic analyzer (ESA) for electrons below 18 keV and two solid-

state telescopes (SST's) for electrons above 16 keV and ions above 50 keV. All detectors point

in the plane of the ecliptic and have an opening angle of about 15° in and ±25° normal to the

ecliptic. The instrument began operation on 14 August 1978 two days after launch and ceased

operation on 22 November 1979. The instrument is also described by *Anderson et al.* [1978].

The ISEE spacecrafts and instruments are described in the same issue of *IEEE Transactions on

Geoscience Electronics.*

Table I-2 shows how the data are telemetered to the earth. Some channels are sectored to

provide angular distributions in the ecliptic. The sectoring was command selectable to be with

respect to either the sun direction or the ecliptic component of the magnetic field. As particles

at these energies have less bulk energy than the magnetic field, the particles, especially elec-

trons, tend to spiral about the magnetic field. Magnetic sectoring was used for most of the mis-

sion.

The "To take" column shows the time to take a sample. For sectored channels, the

numerator is the number of spins to take a sample, the denominator is the number of sectors.

Although a spin takes only three seconds, for telemetry purposed this is expanded into four

seconds. During the four seconds, a spin's worth of data is taken, then the magnetic field

Name	Detector Assembly	Number of Energies	Energy Resolution	Sample times (sec)	
------	-------------------	--------------------	--------------------	To take	Between
SESA	$E_1\bar{E}_p$	16	12%	$T/16$ (.1875)	64
REP	E_p	1		8	8
SOTL	$O_1\bar{O}_2\bar{O}_p$	4	60%	$2T/16$ (.375)	32
O1PHA		22	22%	$64 - SB$	64
SOTH	$O_1O_2\bar{O}_p$	1		$4T/8$ (1.5)	16
O2PHA	$(O_1+O_2)O_1O_2\bar{O}_p$	16	35%	$64 - SB$	64
O2	$\bar{O}_1O_2\bar{O}_p$	1		8	8
CO	$O_1O_2O_p$	1		8	16
SFT	$F_1\bar{F}_p$	4	55%	$2T/16$ (.375)	32
FTPHA		16	20%	64	64
CF	F_1F_p	1		8	16

Table I-2. Telemetry Summary. The second column shows the logical conditions necessary to record a count (bar is for anti-coincidence). The plus in the O2PHA channel is for the arithmetic sum of the pulse heights. T is spacecraft spin period (3s). Channels whose names begin with S are sectored channels—in the sample time, the numerator is the number of spins to take a sample, the denominator is the number of sectors per spin. SB is the time removed for sun blocking (~20%).

reference is updated and the energy changed. The "Between" time is the time between starting samples at the same energy. Thus for the ESA, a spin's worth of data is taken at each energy and time between samples at a given energy is 64 seconds. Actually, we could command the ESA into a mode where every other energy step is skipped so that it takes 32 seconds to cover the entire energy range. This mode was used for less than one week of the instrument lifetime.

For solid-state telescopes more than one energy can be sampled at a time. Nevertheless, the sectored channels are sampled one at a time. At the same time, the pulse heights are sorted into pulse height analyzers (PHA's) with no angular information. Because sunlight produces a large noise pulse, the open telescope PHA's do not count while the detectors view the sun. The foil telescope PHA is not sun-blocked as the foil makes the assembly light tight. However, the detector sees soft solar X-rays and there is a noise pulse almost as large as the light generated pulses in the open telescope. I will discuss the problems this caused later.

Particle counts accumulate in 19 bit counters except for the PHA's which are 16 bits. Counts are compressed into 8 bit words before being telemetered. The compression is to five bits plus a four bit exponent and is accurate to about three percent. Adding the eight house-keeping words to the words shown in the table gives 640 words per 64 seconds or 80 bits/second.
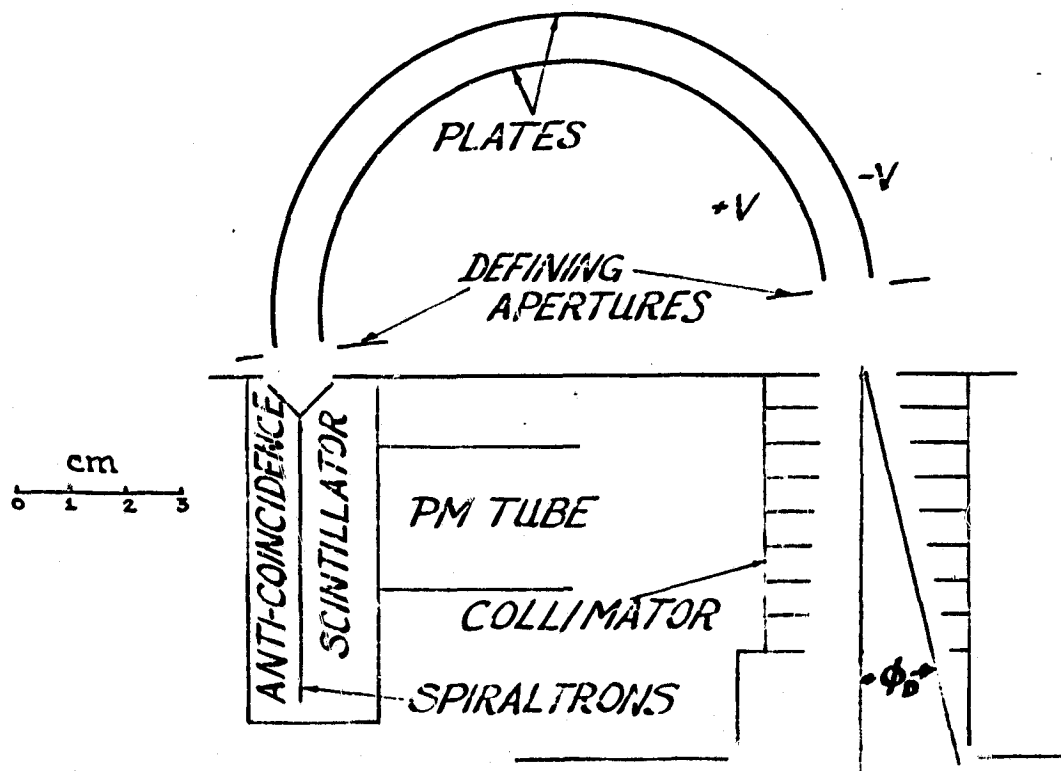
I-B. Electrostatic Analyzer (ESA)

Figure I-2. Schematic of Electrostatic Analyzer.

The electrostatic analyzer (Figure I-2) consists of two hemisphere plates of radii 4.625 cm and 5.375 cm. I define ϕ_D as shown and θ_D as perpendicular to the page. The advantage of hemisphere plates is that the entrance aperture is imaged at the exit aperture and thus detection of a particle that enters the aperture is independent of θ_D. The entrance aperture is about 5 cm by 0.75 cm. The detector is five funnel-mouthed spiral electron multipliers (spiraltrons) with

active area about 1 cm² each. The spiraltrons are imbeded in plastic scintillator for anticoincidence of penetrating cosmic rays.

The analyzer was designed to measure electrons in the energy range 2 - 18 keV in 16 logarithmically spaced steps. As detailed later, we discovered early in the data analysis stage that a malfunction in the high voltage supply limited the upper energy to ~8 keV.

For any detector, the expression for obtaining differential flux J from count rate C is

$$J = \frac{C}{G} \tag{I-1}$$

where the geometric factor G has the dimensions of $A \Omega \Delta E$ where A is the sensitive area, Ω is the solid angle, and ΔE is the energy bandwidth of the detector. For an ESA, whether or not a particle at a particular energy is detected depends on its entrance angle. At a given angle, ΔE is about half of what it is integrated over the entire aperture. For the entire aperture, one expects $\Delta E/E \approx \Delta R/R$ where E is the center energy and R is the average plate radius. Although ΔE is a function of solid angle, G depends only on E (through ΔE) linearly. Thus, I express G as a constant times E.

Although attempts have been made to model the geometric factor of large-aperture electrostatic analyzers, they have never been particularly successful. Initial analysis for an analyzer of this geometry based on *Chase* [1973] indicated that the geometric factor should be ~$0.02 E$ cm²–ster where E is the particle energy and the center response at $\phi_D \approx 1°$.

An electron gun provided electrons to calibrate the energy response. As expected, The energy bandwidth at the center response angle is ~6%. The center response angle is at about $\phi_D \approx -1°$. At a given energy, full-width at half-maximum (FWHM) angular response is about $11° \times 55°$.

For the geometric factor, a ^{63}Ni source supplied an essentially flat spectrum over the relatively small bandwidth of the ESA. A solid-state detector provided an absolute calibration of the source strength. The largest available vacuum chamber provides a maximum path length of

~25 cm and thus the aperture subtends an angle of ~10°. This relatively large angle dictated the use of masks on the entrance aperture. Painstaking measurements over a period of several weeks taken over a large number of angles yielded the approximate response pattern and a geometric factor of ~0.0098 E cm^2–ster.

To reduce response to Lyman-α photons, the outer hemisphere is serrated on the inside to increase the number of reflections necessary to get to the detector and the insides of both plates are coated with gold black to absorb photons. Ultraviolet response is about 0.33 counts/second.

A voltage divider-voltmeter combination measured the voltages on the stepping voltage supply for the ESA. The voltage times the conversion constant 0.00626 keV/V yields the ener-

Channel	Energy (keV)
1	2.00
2	2.31
3	2.66
4	3.08
5	3.53
6	4.20
7	4.80
8	5.57
9	6.40
10	7.40
11	8.54
12	10.02
13	11.52
14	13.35
15	15.41
16	17.63

Table I-3. Electrostatic Analyzer Energies.

gies in Table I-3.

I-C. Solid-State Telescopes (SST's)
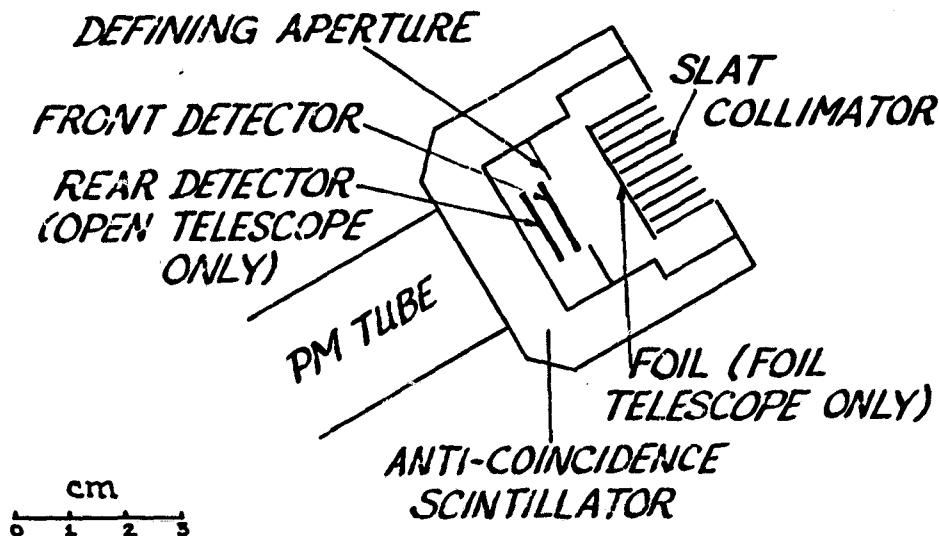
Figure I-3. Schematic of Solid State Telescopes.

All three solid-state detectors (Figure I-3) are surface barrier detectors with active area $\sim 1.5\,cm^2$. To reduce radiation damage, the ohmic contact of aluminum always faces outward. The barrier contact is $\sim 40\,\mu g/cm^2$ of gold. The foil telescope FT consists of a foil covering one $200\,\mu m$ thick detector (F_1). The foil is $220.65\,\mu g/cm^2$ of paralyene $(C_{11}H_{11})$ flashed on both sides with $156.86\,\mu g/cm^2$ aluminum. The front contact of the detector is $120.1\,\mu g/cm^2$ of aluminum. The open telescope OT consists of a $200\,\mu m$ detector (O_1) in front of a $400\,\mu m$ detector (O_2). The barrier contacts are placed together. The front contact is $60.2\,\mu g/cm^2$ of aluminum. All detectors are imbeded in scintillator plastic with phototube detectors for anticoincidence of penetrating cosmic rays.

The advantage of solid-state detectors is that the height of the pulse coming from the detector is a function of the incident particle energy. The relationship is approximately linear. Non-linearities come from energy loss in the detector window and, for ions, losses to collisions with ions in the detector [*Potter and Campbell*, 1978]. Electrons can also be stopped before depositing all their energy (electron straggling). The lowest energy that a solid-state detector can measure is determined by thermal noise. To reduce noise, the detectors are mounted on a

cold plate that is thermally isolated from the spacecraft. This passive cooling method keeps the detectors at ~ −20 ℃.

The foil stops protons with energies < 250 keV. Thus the foil telescope measure electrons above 18 keV and protons above 250 keV. The front detector of the open telescope measures electrons above 16 keV and protons above ~50 keV. Outputs from the front and rear detectors are summed so that electrons that penetrate to the rear detector will have lower pulse heights than protons. As described in detail later, electrons can be separated from protons and other ions by subtraction.

During the instrument calibration cycle a ramp pulser feeds pulses into the telescope preamplifiers with an amplitude that increases with time. With the ramp slope known, I can count the number of pulses in each channel to determine its width. The intercept (position when the

Channel		Energy (keV)	
		Electron	Proton
SFT	1	18.5	262
	2	34.	285
	3	63.5	305
	4	101.	330
FTPHA	1	18.4	270
	2	19.6	272
	3	23.2	275
	4	27.7	280
	5	34.2	287
	6	42.2	294
	7	52.9	301
	8	65.4	309
	9	81.4	317
	10	102.0	329
	11	128.3	345
	12	160.9	360
	13	200.8	390
	14	251.8	430
	15	317.0	475
	16	393.3	540

Table I-4. Foil Telescope Thresholds.

cycle starts) tells me the absolute energies. Table I-4 is the Foil Telescope thresholds and Table I-5a and Table I-5b are the Open Telescope thresholds. Logarithmically spaced

Channel		Energy (keV)	
		Electron	Proton
SOTL	1	14.2	41.5
	2	28.0	58.5
	3	55.9	88.5
	4	89.6	120
O1PHA	1	19.3	47.5
	2	23.8	53.0
	3	29.5	60.0
	4	36.6	68
	5	45.6	77.5
	6	56.9	89
	7	71.4	104
	8	89.1	119
	9	110.3	135
	10	137.6	160
	11	173.6	195
	12	216.4	240
	13	271.5	290
	14	340.6	360
	15	428.0	445
	16	530.6	560
	17	708.0	708
	18		880
	19		1120
	20		1400
	21		1760
	22		2190
	23		2770
	24		3490
	25		4320
	26		5380
	27		6810
	28		8490
	29		10600
	30		13400
	31		15700
	32		17100

Table I-5a. Open Telescope (SFT,O1PHA) Thresholds.

thresholds provide approximately constant energy resolution $\Delta E/E$.

To determine the slope of the ramp, I compared the spectra taken with the instrument PHA's with the spectra taken with the identical detector assembly and 1024 channel analyzer and computed the best slope with a least squares fit.

Channel		Energy (MeV)				
		Electron	Proton	^{2}H	^{3}He	α
O2PHA	1	0.209				
	2	0.295				
	3	0.421				
	4	0.593				
	5	0.850				
	6	1.180				
	7	(1.66)				
	8	(2.31)				
	9	(3.42)				
	10		4.8	6.4		
	11		6.7	6.7		
	12		9.6	9.6		
	13				17.2	
	14				19.0	19.5
	15				27.1	27.1
	16					38.1

Table I-5b. Open Telescope (O2PHA) Thresholds. Numbers in parenthesis are electronic thresholds.

Collimators determine the SST geometry. The slat collimator shown in Figure I-3 and another collimator not shown give an aperture $\sim 15° \times 60°$ - similar to the ESA. As before, (I-1) is the expression for flux. However, for solid-state detectors A and Ω are constant and ΔE is set by pulse height discriminators. Thus, I express G as a constant times ΔE. Electron straggling and geometric factor were determined using a β-ray spectrometer. Geometric factor is $\sim 0.3 \Delta E$ cm^2–ster

Electron Straggling

Unfortunately, even when the electron range is short compared with the size of the detector, electrons may not contribute all their energy to the pulse height. As the energy gets larger and electrons begin to leave the detector, the picture gets considerably more complicated. The particular anti-coincidence scheme has a large effect on the spectrum of pulse heights for a given incident energy. In the case of our telescopes, the situation is further complicated by the double element in the open telescope.

Using the β-ray spectrometer, we took data at four to five energies and with various coin-
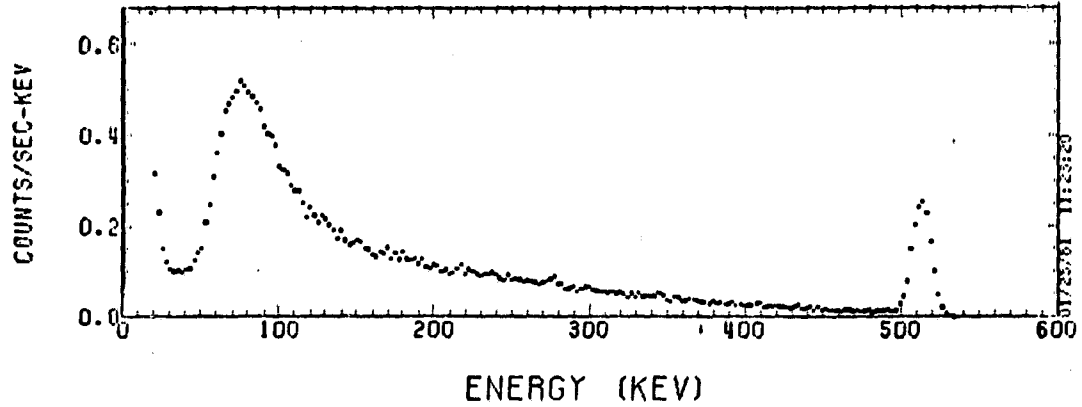
Figure I-4. Response of O1PHA for 514 keV incident electrons.

cidence arrangements for the telescopes (Figure I-4). shows the data from two measurements. At low energies about 85% of the incident electrons leave all of their energy in the detector. The remaining 15% are uniformly distributed over the remaining energies. At higher energies, electrons do not stop in the detector, the peak at the incident energy shrinks and the response at lower pulse heights grows.

Since the pulse heights are naturally binned into channels, I constructed response matrices for each of the three PHA's. By inverting the response matrices, I obtain a transformation from the response spectra to the incident spectra.

II

Data Analysis

II-A. Basic Strategy

Our instrument measures direction flux $J(E,\phi)$ where ϕ is the angle in the ecliptic. The spin averaged flux

$$\bar{J}(E) \equiv \frac{1}{n_s}\sum_s J(E,\phi_s) \tag{II-1}$$

where s is the sector index and n is the number of sectors. Adjunct to this, I define a normalized angular function

$$\eta(E,\phi) \equiv \frac{J(E,\phi)}{\bar{J}(E)} \tag{II-2}$$

which is thus normalized

$$\sum_s \eta(E,\phi_s) = n_s$$

There are several reasons to separate the energy and angular parts. 1) The telescopes already provide spin averaged outputs (the PHA's) with high energy resolution. The angular information comes from different channels. 2) Combining the counts to give $\bar{J}$ gives better statistics for summary plots and spectral deconvolution.

II-B. Summary Plots

The aim of the data analysis program for any satellite must be to present summary plots
of data for all times and detailed analysis for times selected on the the basis of the summary
plots. Thus the summary plots must be brief enough so that they can be scanned in a reason-
able length of time — yet detailed enough to reveal interesting stretches of data, enable
classification, and not hide any significant details. There are two summary plots for each eight
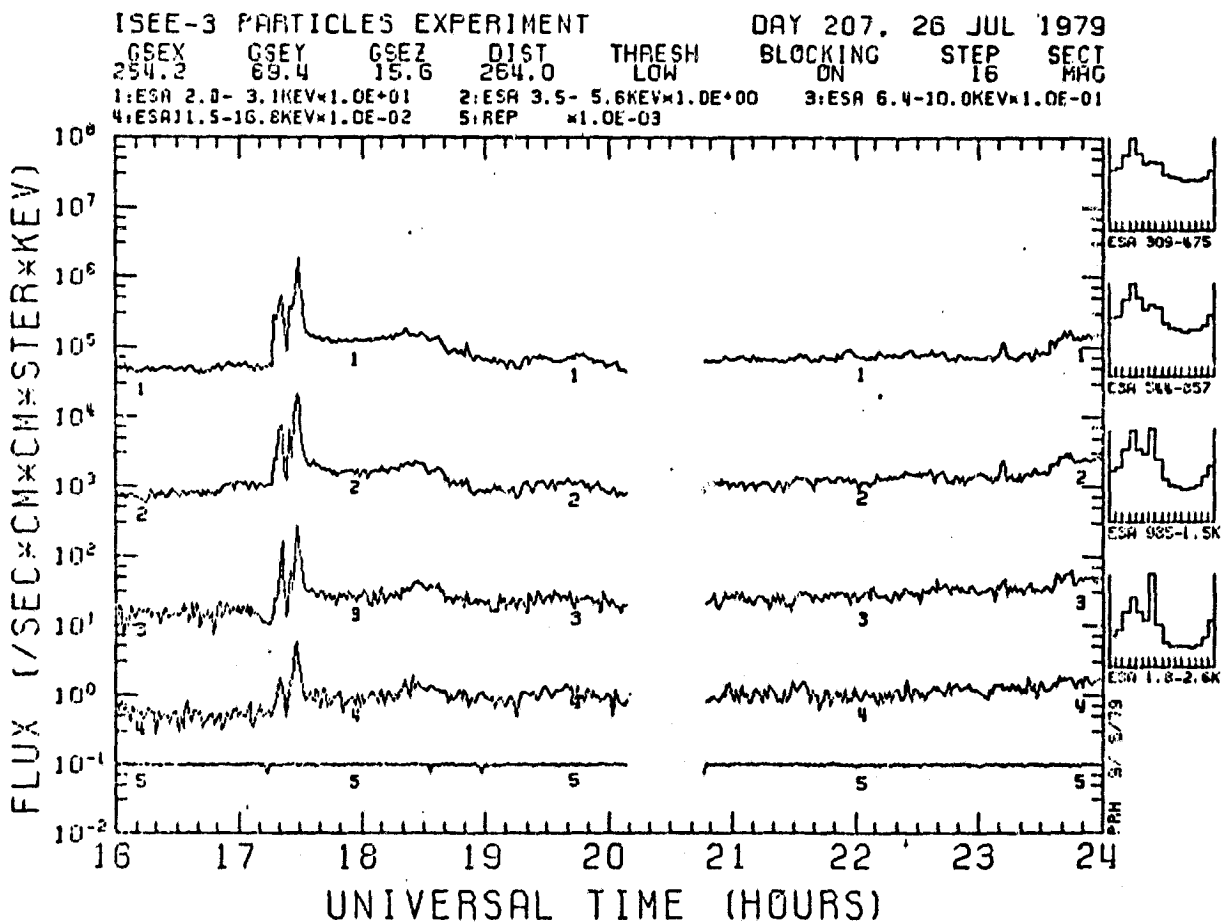
Figure II-1. Sample of Electrostatic Analyzer (ESA) summary plot for 26 July 1979. An interplanetary shock
occurred at 17:25.

hour period - one each for ESA and SST data. On the ESA plot (Figure II-1) are four traces
that represent the average of $\bar{J}$ for 4 energy channels each. The last trace is REP count rate.
REP is sensitive to very high energy particles and gamma rays. It counts at essentially a con-
stant rate (from electronic noise) except during very large flare events, when it can rise by
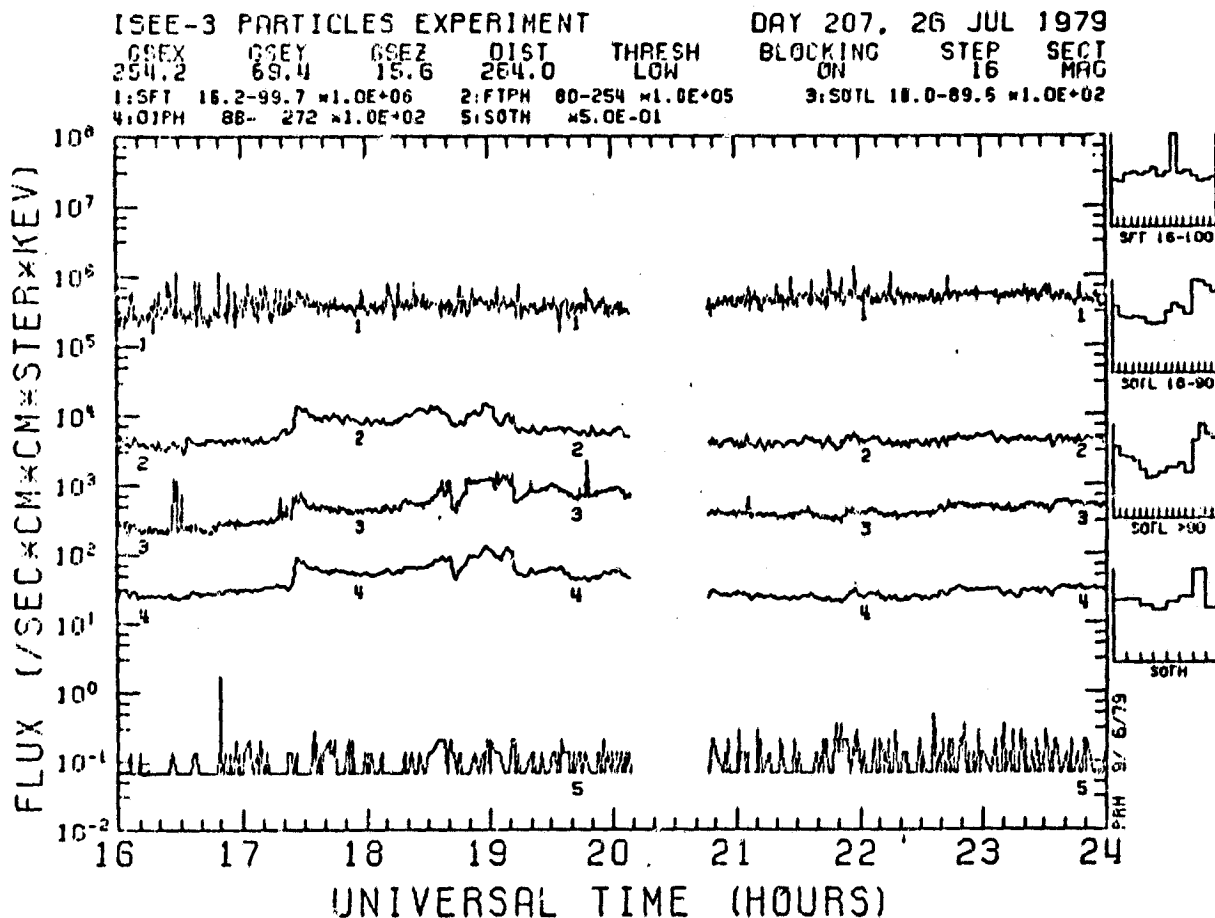
Figure II-2. Sample of Solid-State Telescope (SST) summary plot for the same time period as Figure II-1.

several orders of magnitude. The SST plots (Figure II-2) have one trace each for SFT and

SOTL (the lowest three channels in each case), one trace each for FTPHA and OlPHA (from

where SFT and SOTL leave off up to about 300 keV), and one trace for SOTH count rate. On

the sides of the plots are rough angular histograms.

II-C. Sun Blocking

The presence of large noise pulses in the telescopes when they view the Sun dictates some

sort of corrective processing. In the sectored channels, we do this by removing the sectors that

correspond to the Sun. This is difficult as the sectoring is fixed to the magnetic field and not

the Sun. The spacecraft telemetry provides the position of the Sun with respect to B every 32

seconds — however the sector clock updates every 4 seconds. Since the Sun can shift rapidly, we must recognize the pattern of the Sun in the sectors and eliminate those sectors that are Sun contaminated. [*Harvey*, private communication]

The open telescope PHA's are turned off when the telescopes view the Sun by a circuit within the instrument. We need only correct for the counting time. FTPHA is not blocked at all and the lower 4-8 channels are useless.

II-D. Correction of Count Rate Drop in the Pulse Height Analyzers

Shortly before launch, I was looking over a raw dump of a test cycle and discovered that the PHA readout sometimes dropped a count. The drop appears to be random but happens a high percentage of the time. Statistics taken during test cycles show that the percentage is about 90%. I used this percentage to create a curve (Figure II-3) of apparent *vs.* real count rate. The curve is used to correct every PHA count.

II-E. GSE Coordinate System

In the geocentric solar-ecliptic (GSE) coordinate system (Figure II-4), the earth is the origin, $\hat{z}_{GSE}$ points along the north ecliptic pole perpendicular to the ecliptic, $\hat{x}_{GSE}$ points towards the sun, and $\hat{y}_{GSE}$ points towards dusk. In this system, the solar wind velocity v_{SW} is nominally in the $-x$ direction. The average B is in the $x-y$ (ecliptic) plane with $B_\phi \approx 135°$ or $45°$ (the Parker spiral angle).

II-F. Calculation of the pitch angle

Since the particles tend to spiral around B, a natural way to specify the particle's velocity is with speed v, pitch angle α, and gyrophase Ω. Although magnetic sectoring helps consider-
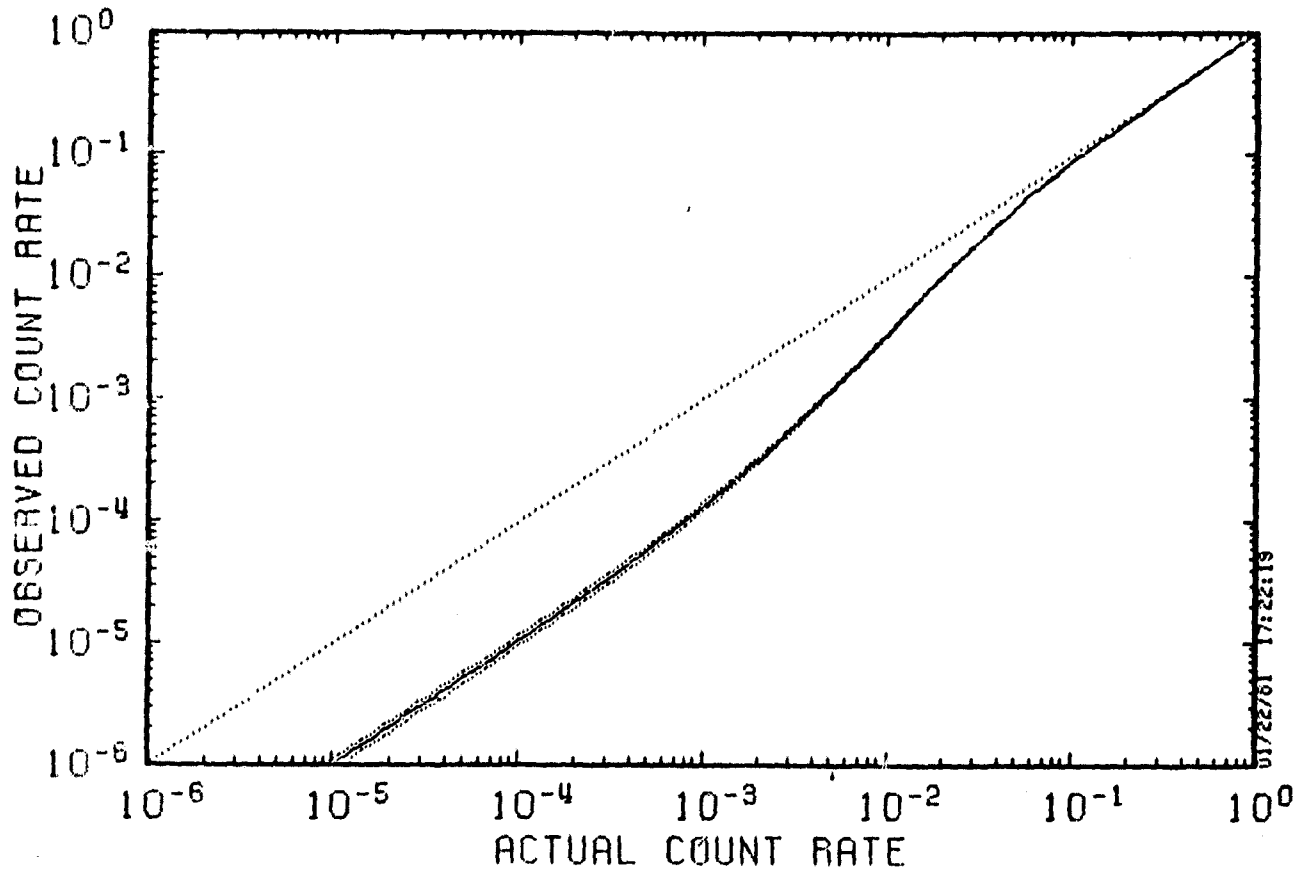
Figure II-3. Apparent *vs.* real count rate for a 64 sec PHA read-out period. A singe count is dropped for a read-out period 90% of the time.

ably, the natural system for the detector is, of course, different. I choose $\hat{z}_D = \hat{z}_{GSE}$ and $\hat{x}_D$ and $\hat{y}_D$ such that **B** is in the $x-z$ plane. Note that the $x-y$ plane is still the ecliptic. For the magnetic coordinate system, $\hat{y}_B = \hat{y}_D$ and $\hat{z}_B \parallel \mathbf{B}$. Note that α and Ω are the polar and azimuthal angles respectively in this system. The transformation between systems is

$$I_{M-D}(\theta_B) = \begin{bmatrix} \cos\theta_B & 0 & \sin\theta_B \\ 0 & 1 & 0 \\ -\sin\theta_B & 0 & \cos\theta_B \end{bmatrix} \tag{II-3}$$

where θ_B is the angle between $\hat{z}_{GSE}$ and **B**.

The detector counts particles when $-\mathbf{v}$ has θ and ϕ within the detector aperture. The complete transformation between velocity and detector is

$$\tan\phi = \frac{-\sin\alpha \sin\Omega}{-\sin\alpha \cos\Omega \cos\theta_B - \cos\alpha \sin\theta_B} \tag{II-4a}$$
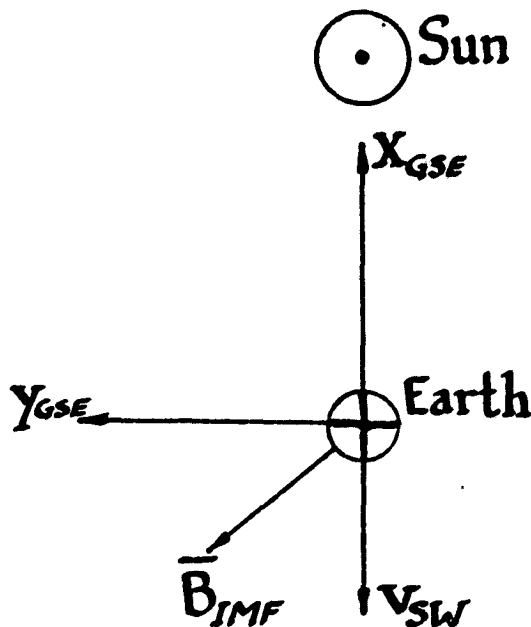
Figure II-4. Geocentric solar ecliptic (GSE) coordinate system in the ecliptic plane. $\hat{z}_{GSE}$ points up out of the page.

$$\cos\theta = \sin\alpha \, \cos\Omega \, \sin\theta_B - \cos\alpha \, \cos\theta_B \qquad \text{(II-4b)}$$

and the inverse transformation is

$$\cos\alpha = -\sin\theta \, \cos\phi \, \sin\theta_B - \cos\theta \, \cos\theta_B \qquad \text{(II-5a)}$$

$$\tan\Omega = \frac{-\sin\theta \, \sin\phi}{-\sin\theta \, \cos\phi \, \cos\theta_B + \cos\theta \, \sin\theta_B} \qquad \text{(II-5b)}$$

I have not cancelled out the signs in the numerator and the denominator of the $\tan^{-1}$ to make

the range the required $360°$.

The detector gives information as to ϕ within the sector size of $22\frac{1}{2}°$ and no information

as to θ except that it is within the detector aperture $\theta = 90 \pm 25°$. For the nominal $\theta_B = 90°$,

$$\cos\alpha = -\sin\theta \, \cos\phi$$
$$\alpha \approx |\, 180° - \phi \,|$$

To actually calculate the pitch angle distribution, I first assume that the particles are uni-

formly distributed in Ω and, for each gyrophase interval, calculate which sector will detect the

particles. Figure II-5 is a plot of response *vs.* α for each sector.
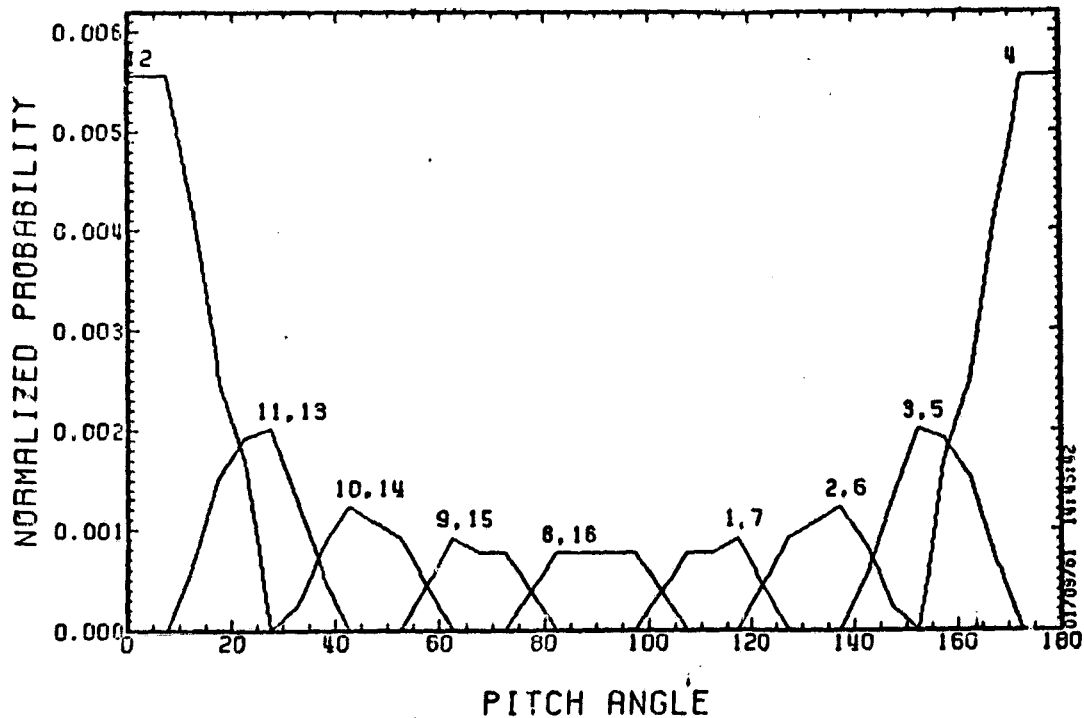
Figure II-5. Response as a function of pitch angle α for each sector of 22½°. Sector 4 corresponds to $-11\frac{1}{4}° < \phi < 11\frac{1}{4}°$.

II-G. Spectral Deconvolution

Recall from the last chapter that the lower channels of O2PHA have electrons above 200 keV, O1PHA has electrons plus protons above ~50 keV, and FTPHA has electrons above 20 keV and protons above 270 keV. Thus O2PHA subtracted from O1PHA yields protons only above 270 keV. These protons subtracted from FTPHA leaves electrons only in FTPHA. These electrons subtracted from O1PHA below 270 keV yields protons below 270 keV.

Further complicating the issue is the electron straggling and efficiency corrections. I lump these corrections into one multiplication by a matrix. Of course, this matrix is different for each PHA. This correction is most easily done on the differential spectra. The differential spectra is the spectra as collected by the instrument. Each channel contains the number of counts between its threshold and the next higher threshold.

The subtraction process is done with integral spectra. In an integral spectrum, each channel contains the number of counts above its threshold. It is simply related to the differential

spectrum $J(E)$,

$$K_i \equiv \sum_{j=i}^{N} J_j$$

Before subtracting PHA_2 from PHA_1, we must recompute the spectrum represented by PHA_2 with the thresholds of PHA_1. We do this with a power law interpolation (straight line on a log-log plot).

Following is the step by step process. O2PHA refers to the lower channels of O2PHA.

1   Correct O2PHA for straggling. O2PHA now has the correct electron spectrum > 200 keV.

2   Convert O2PHA to integral and recalculate spectra for O1PHA electron thresholds. Convert to differential, uncorrect for straggling/efficiency, and convert to integral.

3   Subtract this from the integral O1PHA spectrum > 250 keV. O1PHA now has the correct proton spectrum above 250 keV.

4   Recalculate O1PHA > 250 keV spectrum for FTPHA proton thresholds and subtract from integral FTPHA spectrum.

5   Convert FTPHA to differential and straggling/efficiency correct. FTPHA now has the correct electron spectrum from 20 to 400 keV.

6   Integrate FTPHA, convert to O1PHA electron thresholds, differentiate, uncorrect for straggling/efficiency, integrate, and subtract from O1PHA < 250 keV. O1PHA now has the correct protons spectrum > 50 keV.

II-H. Velocity Distributions

The flux J is related to the velocity-space distribution function f by

$$J(E,\alpha) \, dE \, dA \, d\Omega \, dt = f(\mathbf{x},\mathbf{v}) \, dA \, v dt \, v^2 dv \, d\Omega$$

or

$$f(\mathbf{x},\mathbf{v}) = \frac{m^2}{2E} J(E,\alpha) \tag{II-6}$$

The parallel distribution function $f(v_\parallel)$ is important in that a positive slope leads to growth of plasma waves which may produce Type III radio bursts. It is a projection of f along the field direction.

$$f(v_\parallel) \equiv \int f(v)\, d^2 v_\perp = \tfrac{1}{2} \int f(v)\, v_\perp\, dv_\perp\, d\theta$$

where I have used cylindrical coordinates. Further manipulation gives:

$$f(v_\parallel) = \pi m \int\limits_{\frac{1}{2}mv_\parallel^2}^{\infty} J(E, \cos\alpha = \frac{v_\parallel}{v} = \frac{v_\parallel}{\sqrt{2E/m}})\, \frac{dE}{E}. \tag{II-7}$$

APPENDIX B

The X-Ray Spectrometer Experiment

X-Ray Spectrometer Experiment Aboard the ISEE-C (Heliocentric) Spacecraft

K. A. ANDERSON, S. R. KANE, J. H. PRIMBSCH, R. H. WEITZMANN,
W. D. EVANS, R. W. KLEBESADEL, AND W. P. AIELLO

Abstract–This experiment is designed to provide continuous coverage of solar flare X-ray bursts and transient cosmic gamma-ray bursts. A proportional counter and a scintillation detector together cover the energy range from 5 to 228 keV with good sensitivity, large dynamic range, and high temporal resolution. This experiment provides data storage capability and good absolute timing so that in conjunction with similar experiments on other spacecraft, accurate source locations can be obtained for cosmic gamma-ray bursts.

I. INTRODUCTION

THE University of California X-ray experiment aboard the ISEE-C (Heliocentric) spacecraft has been designed to study two transient astrophysical phenomena, viz. solar flares and cosmic gamma-ray bursts. Although these two phenomena occur on different cosmic scales, they have several common observational features, such as emission of photons > 10 keV with rapid time variations and photon flux which decreases with increase in photon energy.

A. Solar Flares

Many solar flares produce energetic particles over a wide energy range. Acceleration of electrons to a few hundred keV energy occurs during the impulsive phase of a flare. Higher energy electrons, protons, and heavier nuclei are accelerated later in the flare. The total energy of the electrons > 10 keV represents a large fraction of the total energy of the flare [1]. Energetic (> 10 keV) electrons interacting with the ambient ions produce X-rays through bremsstrahlung. Therefore, through hard X-ray measurements, it is possible to deduce the characteristics of the electron acceleration process, such as basic time constant, efficiency, energy spectrum, and total energy of the accelerated electrons.

In the past, hard X-ray measurements suffered from one or more of the following instrumental limitations: pulse pile-up [3], [2] low sensitivity, small dynamic range, inadequate time resolution, or lack of continuous solar coverage. The X-ray experiment on ISEE-C is relatively free of these limitations. It provides 1) continuous coverage of the sun, 2) large dynamic range to cover small as well as large flares, 3) high resolution X-ray spectra in the 5–228 keV range, 4) supplementary photon measurements up to 1.25 MeV, and 5) high time resolution (0.125 s) for 12–132 keV X-rays.

B. Transient Cosmic Gamma-Ray Bursts

The transient cosmic gamma-ray bursts [4] are a relatively new observational phenomenon in high energy astrophysics. These cosmic bursts typically occur at an average rate of one or two per month, have rise times < 1 s, durations ranging from < 1 to ~ 100 s, and substructure with a time scale of > 0.02 s. In order to determine their origin precise directional information is needed so that optical and radio searches can be carried out to identify the sources. Such information can be obtained through long baseline interferometry with a network of properly designed detectors on widely separated spacecraft. The experiment on ISEE-C provides one element of such a network with the following desirable capabilities: 1) full time coverage, 2) nearly omnidirectional field-of-view over approximately 3π str for photons > 130 keV, 3) time resolution down to 0.25 ms, and 4) absolute timing within 1 ms.

II. X-RAY DETECTORS

The experiment consists of two cylindrical X-ray detectors: a xenon filled proportional counter (5–14 keV) and a NaI (Tl) scintillator (12–1250 keV). Schematics of the two detectors and their detection efficiency are shown in Fig. 1.

The two detectors are mounted on a tower located above the top of the ISEE-C spacecraft. The axes of the detectors are coincident with the spin-axis of the spacecraft so that the detector axes are maintained perpendicular to the ecliptic plane. The field of view of the proportional counter, as determined by a magnesium collimator, is $\approx 360°$ in the ecliptic plane and $\approx 10°$ FWHM in a direction perpendicular to the ecliptic. A tantalum collimator, most effective for photons < 100 keV, provides a similar field of view for the scintillator. The solar coverage in each spin period is thus > 90 percent. For cosmic X-rays > 130 keV the scintillator field of view is approximately 3π str.

The principal characteristics of the detectors are presented in Table I. The proportional counter is 1.27 cm in diameter and is filled with a mixture of 97-percent xenon and 3-percent CO_2 to a pressure of one atmosphere. The central part of the counter body is made of 0.51-mm thick beryllium and serves as the X-ray entrance window.

The scintillator consists of a 1.0-cm thick cylindrical shell of NaI (Tl) crystal surrounded on all sides by 0.3-cm thick

PROPORTIONAL
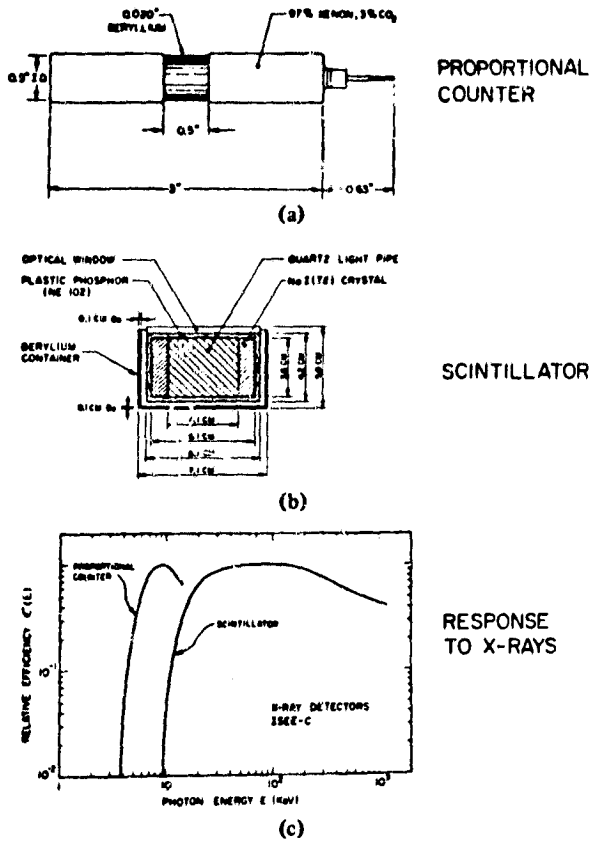COUNTER

(a)

SCINTILLATOR

(b)

RESPONSE
TO X-RAYS

(c)

Fig. 1. (a) Schematic of the proportional counter. (b) Schematic of the scintillator. (c) Relative efficiency of the two detectors for detecting X-rays.

TABLE I
DETECTOR CHARACTERISTICS

DETECTOR TYPE	WINDOW	X-RAY ENERGY RANGE	AREA FOR SOLAR X-RAYS	FIELD OF VIEW	
				IN THE ECLIPTIC PLANE	PERPENDICULAR TO THE ECLIPTIC
Proportional Counter	94 mg cm^{-2} Be	5-14 keV	1.2 cm^2	~360°	~10° FWHM
97% Xenon 3% CO$_2$ Total 1 atm	+6.9 mg cm^{-2} Al	(6 channels)			
NaI(Tl) Scintillator	133 mg cm^{-2} Mg	12-1250 keV	22 cm^2	~360°	~10° FWHM for x-rays <100 keV
	+185 mg cm^{-2} Be	(12 channels)			~300° for x-rays >130 keV

NE-102 plastic scintillator. The central region, which is 4.1 cm in diameter, is filled with a quartz light pipe. Except for an optical window at one end of the cylindrical crystal, the whole scintillator assembly is enclosed in a 0.1-cm thick beryllium container. The scintillator is optically coupled to an EMR 544 S-01-14-20000 photomultiplier tube and is operated in the phoswitch mode so as to reduce the background due to charged particles.

III. ELECTRONICS AND EXPERIMENT OPERATION

The front-end electronics consists of two parallel independent sections. One section provides pulse amplification,

shaping, analysis, and gain control for the proportional counter signals. The other section provides a similar service for the scintillator signals. Additionally, a phoswitch circuit in the scintillator section provides rejection for particle fluxes in the detector by generating a veto pulse whenever a light pulse occurs in the scintillation plastic.

The X-ray energy channels for the two detectors and the corresponding time resolution during different operational modes of the experiment are summarized in Table II. The pulse height analyzer for the proportional counter is a six channel system utilizing stacked discriminators with energy assignments for each channel as shown in the left columns of Table II. The remaining three channels (PC7-PC9) are sums of other channels. The PHA for the scintillator is a 12 channel version of the proportional counter PHA with channel energy assignments shown in Table II. The remaining four channels are sums of other channels.

The experiment has four operational modes, viz. normal, flare-1, flare-2, and gamma-burst. Except for the gamma-burst mode, all data are accumulated in 19-bit floating point accumulators, which are compressed to 8 bits for transmission through the telemetry. The telemetry modes are two, viz. normal and memory read-out (MRO). At the onset of a solar flare, as detected by a rise in count rate above a selected level of certain PHA channels, flare mode logic is activated. The flare-1 mode is intended to supplement the normal telemetry data with a high time resolution (0.125 s) history of a portion of the X-ray spectrum (e.g., 12-132 keV). This time history is stored in a 32K bit semiconductor memory and read out into telemetry after the cessation of solar flare activity. The flare-2 mode is intended to save solar flare spectral information for those solar flares intense enough to interfere with telemetry reception by storing in the memory most of the X-ray spectral information at a reduced time resolution. These data are read-out via telemetry at the end of the flare (MRO mode). During the MRO mode, real time spectral information is transmitted at a reduced rate to allow telemetry space for the memory data.

The gamma-burst mode is triggered when two conditions are satisfied: 1) the count rates of certain PHA channels rise above a selected level and 2) the spectral hardness of incident photons as determined from the ratio of two selected PHA channels (e.g., SC7 and SC2) exceeds a selected value. The second requirement is necessary in order to avoid false triggers during solar flares which usually have a softer spectrum than the cosmic gamma-ray bursts. The SC16 channel data, which have the highest time resolution in this mode, are accumulated in 6-bit scalers. These scalers operate in a fixed time mode at low counting rates and in "time-to-spill" mode at high counting rates. The time resolution therefore varies with the intensity of the cosmic burst. Channels SC7-SC12, which are accumulated over the same time interval but with a reduced time resolution, provide the spectral information.

In case of multiple triggers the priority logic determines the operational mode of the experiment. Since cosmic gamma-ray bursts are a very infrequent phenomenon, the gamma-burst

TABLE II
ISEE-C (HELIOCENTRIC) SOLAR X-RAY SPECTROMETER ENERGY
CHANNELS AND TIME RESOLUTION

Detector	X-Ray Energy Range (keV)	Symbol	Normal Mode (Real Time Data)	Flare-1 Mode Real Time Data	Flare-1 Mode Stored Data	Flare-2 Mode Real Time Data	Flare-2 Mode Stored Data	Gamma Burst Mode Real Time Data	Gamma Burst Mode Stored Data	Memory Read Out Mode (Real Time Data)
Proportional Counter	5.0-6.0	PC1	0.5	0.5	---	0.5	1.0	0.5	---	1.0
	6.0-7.0	PC2	0.5	0.5	---	0.5	4.0	0.5	---	4.0
	7.0-8.5	PC3	0.5	0.5	---	0.5	4.0	0.5	---	4.0
	8.5-10.0	PC4	0.5	0.5	---	0.5	4.0	0.5	---	4.0
	10-12	PC5	4.0	4.0		4.0		4.0	---	
	12-14	PC6	4.0	4.0		4.0		4.0	---	
	5-7	PC7	---	---	0.25*	---	---	---	---	---
	7-10	PC8	---	---	---	---	---	---	---	---
	10-14	PC9	---	---	0.5	---	16.0	---	---	16.0
NaI (Tl) Scintillator	12-20	SC1	0.5	0.5	---	0.5	4.0	0.5	---	4.0
	20-36	SC2	0.5	0.5	---	0.5	4.0	0.5	---	4.0
	36-52	SC3	0.5	0.5	---	0.5	4.0	0.5	---	4.0
	52-68	SC4	0.5	0.5	---	0.5	4.0	0.5	---	4.0
	68-100	SC5	0.5	0.5	---	0.5	4.0	0.5	---	4.0
	100-132	SC6	0.5	0.5	---	0.5	4.0	0.5	---	4.0
	132-164	SC7	0.5	0.5	---	0.5	2.0	0.5	0.004-0.125	4.0
	164-228	SC8	1.0	1.0	---	1.0	2.0	1.0	0.004-0.125	4.0
	228-356	SC9	1.0	1.0	---	1.0	4.0	1.0	0.004-0.125	16.0
	356-484	SC10	2.0	2.0	---	2.0	16.0	2.0	0.004-0.125	16.0
	484-740	SC11	2.0	2.0	---	2.0	16.0	2.0	0.004-0.125	---
	740-1250	SC12	4.0	4.0	---	4.0	---	4.0	0.004-0.125	---
	12-36	SC13	---	---	0.125*	---	1.0*	---	---	0.5*
	36-68	SC14	---	---	0.125	---	1.0	---	---	0.5
	68-132	SC15	---	---	0.125	---	1.0	---	---	0.5
	132*-1250	SC15	---	---	0.125	---	1.0	---	0.00025-0.008	---
Plastic Guard Scintillator		PC	4.0	4.0	1.0	4.0	16.0	4.0	---	16.0

*Could be assigned to another channel by command.
†Telemetry rate 2048 bits/s.

mode has the highest priority (priority 1). Flare-2 and flare-1 modes have priorities 2 and 3, respectively. These assigned priorities can be changed by a ground command.

IV. ON-BOARD CALIBRATION

To maintain spectral stability, the charge gain of each detector can be adjusted by a command to its high voltage power supply (HVPS) or by enabling an automatic source tracking loop (automatic gain control—AGC). In the case of the scintillator, the AGC system is based on the simultaneous emission of an alpha particle and a 60-keV X-ray by an Am^{241} radioactive source. The radioactive source is sandwiched between two small solid-state silicon detectors (SSD). The alpha particles are detected by the SSD and X-rays are detected by the scintillator. Pulses corresponding to alpha particles are gated into the PHA to veto the analysis of any X-ray coincident with the alpha particle emission so as to avoid spectrum contamination by the radioactive source.

The proportional counter uses a similar AGC system (without the coincident alpha particle veto) based on 22-keV X-rays from a Cd^{109} source. Here spectral contamination is avoided by choosing an X-ray source outside the normal energy range (5–14 keV) of the detector.

An analog test pulse generator provides on command a fixed program of pulses into each of the preamp inputs for the purpose of performing onboard testing of the front-end electronics. A digital test pulse generator inserts, on command, logic pulses into the data stream at the output of the PHA's for purposes of testing the accumulation and timing logic downstream.

REFERENCES

[1] K. A. Anderson, S. R. Kane, and R. P. Lin, "Fast electrons from solar flares," presented at the Int. Sem. on the Problem of Cosmic Ray Generation on the Sun, Leningrad, U.S.S.R., 1970.
[2] D. W. Datlowe, *Space Sci. Instrum.*, vol. 1, p. 389, 1975.
[3] S. R. Kane and H. S. Hudson, *Solar Phys.*, vol. 14, p. 414, 1970.
[4] R. W. Klebesadel, I. B. Strong, and R. A. Olson, *Astrophys. J.*, vol. 182, p. 685, 1973.

APPENDIX C

Description of the Electronics

Space Sciences Laboratory
University of California
Berkeley, California 94720

Solar X-ray Spectrometer for the

ISEE-C (Heliocentric) Spacecraft

Description of Electronics

Principal Investigator: Dr. Kinsey A. Anderson
Professor of Physics

Address: Space Sciences Laboratory
University of California
Berkeley, California 94720

Telephone: (415) 642-1313

Co-Experimenter: Dr. Sharad R. Kane
Associate Research Physicist

Address: Space Sciences Laboratory
University of California
Berkeley, California 94720

Telephone: (415) 642-1149

Electronics Engineer: J. Henry Primbsch
Electronics Engineer

Address: Space Sciences Laboratory
University of California
Berkeley, California 94720

Telephone: (415) 642-1974

August 5, 1975

TABLE OF CONTENTS

ISEE-C (Heliocentric) Solar X-ray
Spectrometer Electronics

1.   General Description

In this experiment, solar X-rays in the range of 6 keV to 20 keV
are detected with a gas-filled proportional counter and X-rays in the
range of 12 keV to 1.25 MeV are detected with a phoswitch detector con-
sisting of a NaI (Tl) crystal surrounded by scintillation plastic and viewed
by a photomultiplier tube. The charge pulses from these detectors are
amplified, shaped, and routed to pulse height analyzers (PHA's) for
spectral analysis. Details about the X-ray energy channels and the time
resolution obtained in the different operational modes are presented in
Table I.

To maintain spectral stability, the charge gain of each detector
can be adjusted by a command to its high voltage power supply (HVPS)
or by enabling an automatic source tracking loop (automatic gain control).

Various portions of the spectrum are read out into the space-
craft telemetry link at different rates commensurate with the scientific
objectives of this experiment. Distribution of real time and stored data
in different telemetry formats is shown in Table II.

At the onset of a solar flare, as detected by a rise in count rate
above a selected level of certain PHA channels, Flare Mode logic is
activated. The Flare I mode is intended to supplement the normal tele-
metry data with a high time resolution (0.125 sec) history of a portion of

the X-ray spectrum. This time history is stored in a semiconductor memory and read out into telemetry after the cessation of solar flare activity. The Flare II Mode is intended to save solar flare spectral information for those solar flares intense enough to interfere with telemetry reception by storing in the memory most of the X-ray spectral information at a reduced time resolution. These data are read out via telemetry at the end of the flare.

During the memory read out mode (MRO), real time spectral information is transmitted at a reduced rate to allow telemetry space for the MRO data.

Built-in test generators allow onboard testing of most of the analog and digital circuitry on command.

2.0   Front End Electronics

The Front End Electronics block diagram is shown in Figure 1 (Diag. ISEE-CX-006); it consists of two parallel independent sections. One section provides pulse amplification, shaping, analysis and gain control for the proportional counter signals. The other section provides a similar service for the scintillation detector signals. Additionally, a phoswich circuit in the scintillation detector section provides rejection for particle fluxes in the detector by generating a veto pulse whenever a light pulse occurs in the scintillation plastic.

The test pulse generators are common to both sections and are programmed to apply stimulus to only one section at a time, thus assuring partial continuity of X-ray data.

2.1 Proportional Counter Section

2.1.1 Preamplifier

Due to the charge gain in the gas fill of a proportional counter, the noise requirements for the charge sensitive preamp are modest compared to the requirements for a solid state detector system covering the same energy range. The amplifier block labeled CSA in the block diagram contains a preamp, shaping network, and a post amplifier.

2.1.2 Automatic Manual Gain Control

The automatic gain control system is based on the simultaneous emission of an alpha particle and an X-ray by a radioactive substance such as Am^{241}. The radioactive material is deposited on or embedded in a small solid state silicon detector. Since the alpha particle energy is approximately 5 MeV, only a modest preamplifier is required to achieve a reasonable signal-to-noise ratio. A lower level discriminator generates a logic pulse for each alpha emission. Via a command bit, this logic pulse is gated into the PHA to veto the analysis of any X-ray coincident with the alpha particle emission to avoid spectrum contamination by the radioactive source. Via a second command bit, this pulse also strobes the output from a window discriminator pair into an up-down counter in the following manner: Every source-coincident pulse from the proportional counter that is above the threshold between the window pair will cause the up-down counter to decrement one count, whereas every coincident pulse below that threshold, but above system noise level, will cause the

up-down counter to increment one count. From geometric considerations, less than half of the coincident X-rays will be detected, but neither these misses, nor the gradual decrease in count rate due to radioactive decay will have any effect on the gain.

The output of the up-down counter drives a digital-to-analog converter (DAC) and the resultant DC output controls the high voltage DC power supply and thus the detector gain.

This AGC loop servoes the system gain tc place the median of the X-ray source spectrum at the common threshold between the two window circuits.

The up-down counter can be preset to any state, and the loop disabled by command to provide for fixed gain control.

2.1.3 HVPS

The high voltage power supply is basically a high voltage amplifier where the output voltage is a large multiple (500 typically) of the input or control voltage. Two systems that have been successfully employed for this purpose at SSL are the following: (a) A class C tuned oscillator with a high voltage secondary winding. An operational amplifier compares the control input with the voltage from a tapped resistor connected across the high voltage output and supplies power as needed to the oscillator circuit. (b) A fixed amplitude oscillator circuit connected to a (tuned) high voltage transformer through an A-C series pass network. An operational amplifier drives the pass network after comparing the input with

the feedback signal as in (a). The operating voltage for a proportional

counter is typically 2000 ± 500 volts.

2.1.4 PHA

The pulse height analyzer for the proportional counter section

is a six channel system utilizing stacked discriminators and trailing edge

logic with energy assignments for each channel as shown in the left

columns of Table I. The remaining two channels are sums of other

channels, i.e., Channel 7 is the sum of Channels 1 and 2, while Channel 8

is the sum of Channels 3 and 4. This summing operation could be con-

sidered part of the downstream electronics.

2.2 Scintillation Counter Section

The scintillation counter section is similar to the proportional

counter section with the exception of a phoswich circuit and a larger num-

ber of channels in the PHA.

2.2.1 Preamplifier

As with the proportional counter, the detector gain is substantial,

thus alleviating the need for a very low noise charge sensitive preamplifier.

A primary consideration for the preamplifier is the short decay time of

the plastic scintillator in the phoswich detector. This decay time is

typically 5 nanoseconds as compared to 0.25 microseconds for NaI(Tl)

detectors. In order for the phoswich circuit to achieve a high sensitivity

to the fast rise plastic pulses, which are coincident with the slower NaI (Tl) pulses, the charge sensitive preamplifier must have a rise time capability of 10 nanoseconds or better.

2.2.2 Phoswich

The purpose of surrounding the X-ray detector, a crystal of NaI(Tl), with scintillation plastic is to reject those pulses which are caused by particles, (primarily electrons and protons) and thus avoid the spectral contamination due to these particles traversing the NaI (Tl) crystal. The scintillation plastic is relatively transparent to X-rays so they can readily reach the NaI (Tl) crystal. Particles, however, lose considerable amounts of energy as they traverse the plastic and the resultant fast light flash is detected as a fast rise component of the overall pulse at the charge sensitive preamplifier output. This fast rise component is detected with a phoswich discriminator circuit which must be able to discriminate between a plastic pulse and the normal statistical noise present in the NaI (Tl) pulse due to the photoelectric conversion process at the photocathode. The phoswich discriminator output pulse is routed to the veto input of the PHA and its rate is monitored as PG (Table I). Several detection methods are under investigation at SSL at the time of this writing (30 July 1975) to determine what tradeoffs must be made.

2.2.3   AGC

The automatic gain control system is identical to the one serving the proportional counter.

2.2.4   HVPS

The high voltage power supply for the scintillation detector is servo controlled as in the proportional counter section. The supply must operate a voltage divider string for the photomultiplier dynodes or must otherwise have multiple taps available to power the dynodes. Additionally, it may be necessary to provide a means of limiting the cathode current to protect the photomultiplier tube from damage during extreme solar flares. The operating voltage for a photomultiplier is typically 1500 ± 500 volts.

2.2.5   Pulse Height Analyzer

The PHA for the scintillation detector section is a 12 channel version of the proportional counter PHA with channel energy assignments shown in Table I . Channel 13 is the sum of Channels 1 and 2, Channel 14 is the sum of Channels 3 and 4, and Channel 15 is the sum of Channels 5 and 6. The count rates in the lower channels can be expected to reach or exceed 10^5 counts/second, thus necessitating a careful examination of pulse shaping effects on pulse pileup and spectral distortion.

2.3   Analog Test Pulse Generator

The analog test pulse generator provides a fixed program of pulses into each of the preamp inputs for the purpose of performing onboard testing of as much of the front end electronics as possible, up to and including measuring each channel edge of the PHA's.   Other tests might be system noise tests, AGC window tests, and crosstalk checks.

2.4   Digital Test Pulse Generator

The digital test pulse generator inserts logic pulses into the data stream at the output of the PHA's for purposes of testing the accumulation and timing logic downstream.   It will also be used for testing the flare mode logic and, to some extent, the memory itself.

3.0   Data Handling Electronics

The condensed block diagram for the data handling electronics is shown in Figure 2.   Details are shown in Figure 3 (drawing No. ISEE-CX-005).

Spectral data in the form of PHA output pulses are accumulated in two sets of accumulators.   One set of accumulators (Acc. 1 through 20 in the diagram) are dedicated to accumulating data and reading them out directly into telemetry while the other set of accumulators (21 through 40) are dedicated to the two flare modes for storing data in the memory. Accumulators Nos. 7, 21, 22 and 23 are shared by both systems since it is not necessary for their data to be handled simultaneously in the two separate systems.

A timing signal generator provides control of the accumulation
time of the various accumulators, while two multiplex control logic
blocks provide control of the accumulator readouts into the telemetry
bit stream and into the memory. A memory readout control logic block
provides control of the memory readout into the telemetry bit stream
via the real time multiplex control logic which incorporates some real
time data along with the memory readout.

The internal organization of the memory section is not necessarily
as shown in the block diagram. However, the interfacing has been defined
and is as shown. The memory block as shown in the block diagram ISEE-
HX-005 will be supplied to SSL by the Los Alamos Scientific Laboratory.

3.1   The 623 Floating Point Processor

The 623 unit is a P-MOS LSI chip that will be supplied by NASA-
GSFC. It is used in this experiment as a 19-bit accumulator which,
upon receipt of a timing signal (T.S.), converts the 19-bit count into an
eight bit floating point number. This number is stored in an output shift
register where it can be read out by applying shift pulses. The shift
register has a serial input pin so that many units can be cascaded. The
enormous "wired-or" shown in the block diagram may consist of a com-
bination of such serial chains.

After conversion, the accumulator is cleared and accumulation is
resumed. However, the previous data must be shifted out before the
next conversion to avoid loss of data.

The time intervals between timing signals are the accumulation times listed in Table I as time resolution for the various accumulators and modes. It is to be noted that Table I lists the time intervals for a telemetry rate of 2048 bits/sec. The real time data intervals are scaled directly with bit rate for different bit rates while the Flare Mode time intervals remain unchanged.

3.2   Real Time Multiplex Control

This logic block provides the routing for telemetry shift pulses to the accumulator being read out according to a predetermined format. An example of such a format is shown in Table III. This format satisfies the accumulation and readout times specified in Table I with the addition of one housekeeping readout in each minor frame. There are eight of these housekeeping registers. Four of these housekeeping registers are accumulators which monitor the total count rates in the front end electronics and the other four are registers for reading out (TBD) digital housekeeping functions.

Timing signals and word gates are utilized to direct the shift pulse routing to each accumulator.

During MRO, the logic block switches to a different format, such as shown in Table IV, upon receipt of a MRO flag from the memory readout control block. This MRO flag also causes the timing signal generator to supply longer timing signals to the accumulators in order to reduce the real time readout rate and thus allow telemetry space for the MRO data.

3.3   Flare Mode Multiplex Control

This block provides a dual format function similar to the real time multiplex control. However, it has several additional tasks.

The count rates of selected channels (TBD) are continuously monitored in this block and when the rates exceed a preset level, a Flare I flag is transmitted to the memory and the data corresponding to Flare I in Table I is formatted according to Table V.

If the monitored rates exceed a second preset level, the Flare II flag is sent to the memory and the Flare II data format (Table I and Table VI) is generated and transmitted to the memory.

When the monitored rates drop below a third preset level, the flare status flag to the MRO control block is dropped, allowing this block to initiate a MRO if the memory is full.

The three rate criteria are preset into the flare mode logic by command.

The memory is organized as data blocks consisting of fifteen 16-bit bytes (or thirty 8-bit words). For every sixteen blocks, a header consisting of 16 bytes containing time and status data is generated for a file length of 512 8-bit words. The memory contains eight of these files or 128 blocks. To reduce potential ambiguities during MRO, each 30-word block includes a block counter readout. A divide-by-fifteen circuit advances the block every time fifteen 16-bit transfers have been made. The complete memory format is presented in Table VII.

3.3.1   Flare I Mode

The flare mode accumulators are normally maintained in the Flare I Mode condition and the data are shifted out through a Flare I delay (a shift register) into the flare mode multiplex control.   The delay stores 1 to 2 seconds of data so that when Flare I Mode is triggered, the 1 to 2 seconds of data prior to the trigger are read into the memory. Unless Flare II is triggered, the Flare I data continues until the memory is full (137 seconds).

3.3.2   Flare II Mode

When the Flare II Mode is triggered, the following events take place: Since some timing intervals for Flare II data are as long as 16 seconds, the flare mode timing signal generator is reset so that all accumulations commence with the beginning of the Flare II Mode.   If the memory contains only Flare I data, the memory address is reset and previously stored Flare I data is overwritten with Flare II data until the memory is full (approximately nine minutes). Previously stored Flare II data are not overwritten and no data is accepted by the memory.

3.4   Memory Input

Since the memory is configured to accept 16-bit transfers, the flare mode multiplexer formats all flare data into 8-bit word pairs as shown in Tables V and VI.

The PHA pulse outputs from the scintillation detector channels 7

through 12 and the PG pulse are also routed to the memory for processing of special events having a "hard" or flat X-ray spectrum in contrast to the "soft" or steep spectra of normal solar flares. These special events are rare and take priority over Flare I and Flare II data. The "flatness" characteristic of these events is tested by comparing the count rate of the SC7 channel with the rate of the SC1 channel in the SC1, 7 ratio logic block. When the ratio exceeds a preset level, a ratio flag is sent to the priority logic within the memory system and the transfer to the special event mode is made.

Whenever the memory commences to store data, the MRI avail. flag drops and remains low until the memory data has been read out. The purpose of this flag is to prohibit both of the test pulse generators from being inadvertently triggered on during any data storage mode.

An additional line labeled "test mode" indicates to the memory logic that the test pulse generators are on and to ignore any flare flags that may occur as a result of test data.

3.5   Memory Output

The memory contents are read out as 16-bit bytes under the direction of the MRO control logic after receipt of the correct flare status and MRO avail. flags. The data are shifted into a 16-bit register from which the real time multiplexer shifts 8 bits at a time into the telemetry bit stream according to Tables IV and VII.

3.6 Timing Signals and Slave Clock

The timing signals utilized by the real time accumulation and
readout logic must be synchronized to the telemetry format to effect an
unambiguous transfer of data. The minor frame spike provides a minor
frame synchronism. However, since the normal real time data cycle
extends over eight minor frames, a major frame synchronism is also
necessary. At 512 bits/sec, the major frame spike occurs every 8.53
minutes. This can be uncomfortably long in many cases since the house-
keeping and other subplexed data could be meaningless for up to that length
of time.

The slave clock data contains all of the necessary telemetry infor-
mation for synchronization, and the complete clock data is transferred
at 0.5-second intervals. Consequently, synchronism can be established
within 0.5 second at any bit rate or time. The bit rate flags from the
spacecraft telemetry system are used as pointers to indicate the proper
set of bits to use for synchronism in the slave clock data.

3.7 Command System

The 37-bit serial command from the spacecraft is shifted through
a (TBD) length shift register and loaded into a holding register at the
trailing edge of the command envelope pulse. The command bits are
distributed as needed from the holding register to the various parts of
the experiment.

3.8   Analog Multiplexer

The analog multiplexer switches the (TBD) internal housekeeping signals into two data lines. The inputs to the multiplexer must be arranged such that one of the output lines can never be less than 0.5 volt above ground when the experiment is operating, since this line will be used as a power-on flag.

Table I

ISEE-C (HELIOCENTRIC) SOLAR X-RAY SPECTROMETER

ENERGY CHANNELS AND TIME RESOLUTION

Detector	Final[+] ray Energy Range (keV)	Symbol	Normal Mode (Real Time Data)	Flare-1 Mode Real Time Data	Flare-1 Mode Stored Data	Flare-2 Mode Real Time Data	Flare-2 Mode Stored Data	Memory Read Out Mode (Real Time Data)
Proportional Counter	5.0-6.0	PC1	0.5	0.5	---	0.5	1.0	1.0
	6.0-7.0	PC2	0.5	0.5	---	0.5	4.0	4.0
	7.0-8.5	PC3	0.5	0.5	---	0.5	4.0	4.0
	8.5-10.0	PC4	0.5	0.5	---	0.5	4.0	4.0
	10-12	PC5	4.0	4.0		4.0		
	12-14	PC6	4.0	4.0		4.0		
	5-7	PC7	---	---	0.25*	---	---	---
	7-10	PC8	---	---	---	---	---	---
	10-14	PC9	---	---	0.5	---	16.0	16.0
NaI (Tl) Scintillator	12-20	SC1	0.5	0.5	---	0.5	4.0	4.0
	20-36	SC2	0.5	0.5	---	0.5	4.0	4.0
	36-52	SC3	0.5	0.5	---	0.5	4.0	4.0
	52-68	SC4	0.5	0.5	---	0.5	4.0	4.0
	68-100	SC5	0.5	0.5	---	0.5	4.0	4.0
	100-132	SC6	0.5	0.5	---	0.5	4.0	4.0
	132-164	SC7	0.5	0.5	---	0.5	2.0	4.0
	164-228	SC8	1.0	1.0	---	1.0	2.0	4.0
	228-356	SC9	1.0	1.0	---	1.0	4.0	16.0
	356-484	SC10	2.0	2.0	---	2.0	16.0	16.0
	484-740	SC11	2.0	2.0	---	2.0	16.0	---
	740-1250	SC12	4.0	4.0	---	4.0	---	---
	12-36	SC13	---	---	0.125*	---	1.0*	0.5*
	36-68	SC14	---	---	0.125	---	1.0	0.5
	68-132	SC15	---	---	0.125	---	1.0	0.5
Plastic Guard Scintillator		PG	4.0	4.0	1.0	4.0	16.0	16.0
Frame Counter		---	---	---	1.0	---	4.0	
Total Bits/sec			208.0	208.0	256.0	208.0	64.0	80.0

Time Resolution (sec)[+]

[+] Telemetry rate 2048 bits/sec.

*Could be assigned to another channel by command:

CMD 6 Bit 4 (25 SEL)
0 = PC7
1 = PC8

CMD 6 Bit 2   Bit 3 (21 SEL)
0   0 - SC13
1   0 = SC 2
0   1 = SC 7
1   1 = SC 8

[+] Exact values depending on the detector gain set by command.

(30 July 1975)

Table II

DISTRIBUTION OF REAL TIME AND STORED DATA

IN DIFFERENT TELEMETRY FORMATS

Telemetry Format	Average Bits Per Minor Frame			
	Real Time Data	Stored Data	Experiment Status	Total
Normal	104	---	8	112
Flare-1	104	---	8	112
Flare-2	104	---	8	112
Memory Readout	40	64	8	112

Table III   – 67 –   18.

NORMAL MODE REALTIME DATA FORMAT (EXAMPLE)

ISFE-C (HELIOCENTRIC) SOLAR X-RAY SPECTROMETER

0.5 SEC
MINOR FRAME

4.0 SEC
DATA CYCLE

PC1	PC2	PC3	PC4	SC1	SC2
SC3	SC4	SC5	SC6	SC7	SC8
PC5	H1				

PC1	PC2	PC3	PC4	SC1	SC2
SC3	SC4	SC5	SC6	SC7	SC9
PC6	H2				

PC1	PC2	PC3	PC4	SC1	SC2
SC3	SC4	SC5	SC6	SC7	SC8
SC10	H3				

PC1	PC2	PC3	PC4	SC1	SC2
SC3	SC4	SC5	SC6	SC7	SC9
SC11	H4				

PC1	PC2	PC3	PC4	SC1	SC2
SC3	SC4	SC5	SC6	SC7	SC8
SC12	H5				

PC1	PC2	PC3	PC4	SC1	SC2
SC3	SC4	SC5	SC6	SC7	SC9
PG	H6				

PC1	PC2	PC3	PC4	SC1	SC2
SC3	SC4	SC5	SC6	SC7	SC8
SC10	H7				

PC1	PC2	PC3	PC4	SC1	SC2
SC3	SC4	SC5	SC6	SC7	SC9
SC11	H8				

Table IV – 68 –　19.

MRO MODE DATA FORMAT (EXAMPLE)

ISEE-C (HELIOCENTRIC) SOLAR X-RAY SPECTROMETER

0.5 SEC MINOR FRAME

4.0 SEC
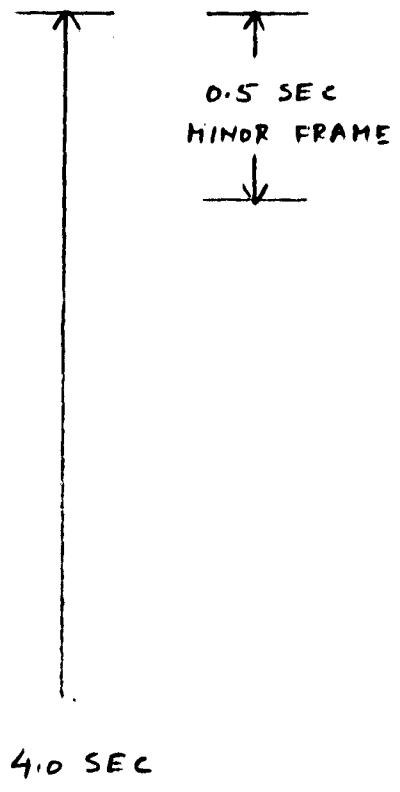
MRO1	MRO2	MRO3	MRO4	MRO5	MRO6
MRO7	MRO8	SC1	SC13	SC14	SC15
PC1	H1				

MRO9	MRO10	MRO11	MRO12	MRO13	MRO14
MRO15	MRO16	SC2	SC13	SC14	SC15
PC2	H2				

MRO17	MRO18	MRO19	MRO20	MRO21	MRO22
MRO23	MRO24	SC3	SC13	SC14	SC15
PC1	H3				

MRO25	MRO26	MRO27	MRO28	MRO29	MRO30
MRO31	MRO32	SC4	SC13	SC14	SC15
PC3	H4				

MRO33	MRO34	MRO35	MRO36	MRO37	MRO38
MRO39	MRO40	SC5	SC13	SC14	SC15
PC1	H5				

MRO41	MRO42	MRO43	MRO44	MRO45	MRO46
MRO47	MRO48	SC6	SC13	SC14	SC15
PC4	H6				

MRO49	MRO50	MRO51	MRO52	MRO53	MRO54
MRO55	MRO56	SC7	SC13	SC14	SC15
PC1	H7				

MRO57	MRO58	MRO59	MRO60	MRO61	MRO62
MRO63	MRO64	SC8	SC13	SC14	SC15
*	H8				

* THIS WORD IN EVERY 8TH MINOR FRAME IS SHARED AMONG PC 5+6, SC9, SC10, AND PG.

Table V

FLARE I MODE DATA FORMAT TO MEMORY

ISEE-C (HELIOCENTRIC) SOLAR X-RAY SPECTROMETER

1.0 SEC

SC 13	SC 14
SC 15	SC 13
SC 14	SC 15
PC 7	SC 13
SC 14	SC 15
SC 13	SC 14
SC 15	PC 7
SC 13	SC 14
SC 15	SC 13
SC 14	SC 15
PC 7	SC 13
SC 14	SC 15
SC 13	SC 14
SC 15	PC 7
P G	BLK#
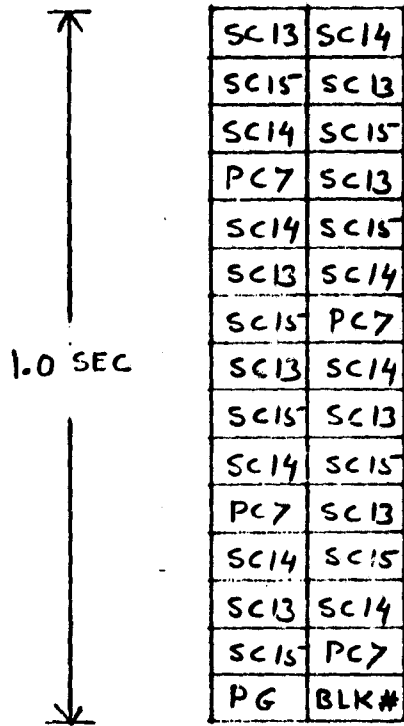
ONE MEMORY BLOCK (30 8-BIT WORDS) OF FLARE I. DATA

ALL 128 BLOCKS FOLLOW THIS FORMAT

FLARE II MODE DATA FORMAT TO MEMORY

ISEE-C (HELIOCENTRIC) SOLAR X-RAY SPECTROMETER

	BLOCK 1		BLOCK 2		BLOCK 3		BLOCK 4	
4.0 SEC	PC1	SC13	PC1	SC13	PC1	SC13	PC1	SC13
	SC14	SC15	SC14	SC15	SC14	SC15	SC14	SC15
	PC2	PC3	PC2	PC3	PC2	PC3	PC2	PC3
	PC4	SC1	PC4	SC1	PC4	SC1	PC4	SC11
	PC1	SC13	PC1	SC13	PC1	SC13	PC1	SC13
	SC14	SC15	SC14	SC15	SC14	SC15	SC14	SC15
	SC2	SC3	SC2	SC3	SC2	SC3	SC2	SC3
	SC4	SC5	SC4	SC5	SC4	SC5	SC4	SC5
	PC1	SC13	PC1	SC13	PC1	SC13	PC1	SC13
	SC14	SC15	SC14	SC15	SC14	SC15	SC14	SC15
	SC6	SC7	SC6	SC7	SC6	SC7	SC6	SC7
	SC8	SC9	SC8	SC9	SC8	SC9	SC8	SC9
	PC1	SC13	PC1	SC13	PC1	SC13	PC1	SC13
	SC14	SC15	SC14	SC15	SC14	SC15	SC14	SC15
	PC 5+6	BLK 1	SC10	BLK 2	SC11	BLK 3	PG	BLK 4

BLOCKS 5–128 ARE REPETITIONS OF THE ABOVE 4-BLOCK FORMAT.

Table VII

MEMORY FORMAT

ISEE-c (HELIOCENTRIC) SOLAR X-RAY SPECTROMETER

$$\begin{bmatrix} \text{TOTAL MEMORY} = 2048 \quad 16\text{-BIT WORDS} \\ \text{ONE MEMORY FILE} = 256 \quad 16\text{-BIT WORDS} \end{bmatrix}$$

| HEADER | 16 | 16-BIT WORDS |

| BLOCK NO. 1 | 15 | 16-BIT WORDS |

MEMORY FILE NO. 1

| BLOCK NO. 16 | 15 | 16-BIT WORDS |

| HEADER | 16 | 16-BIT WORDS |

MEMORY FILE NO. 2

| BLOCK NO. 32 | 15 | 16-BIT WORDS |

MEMORY FILE NO. 8

| BLOCK NO. 128 | 15 | 16-BIT WORDS |
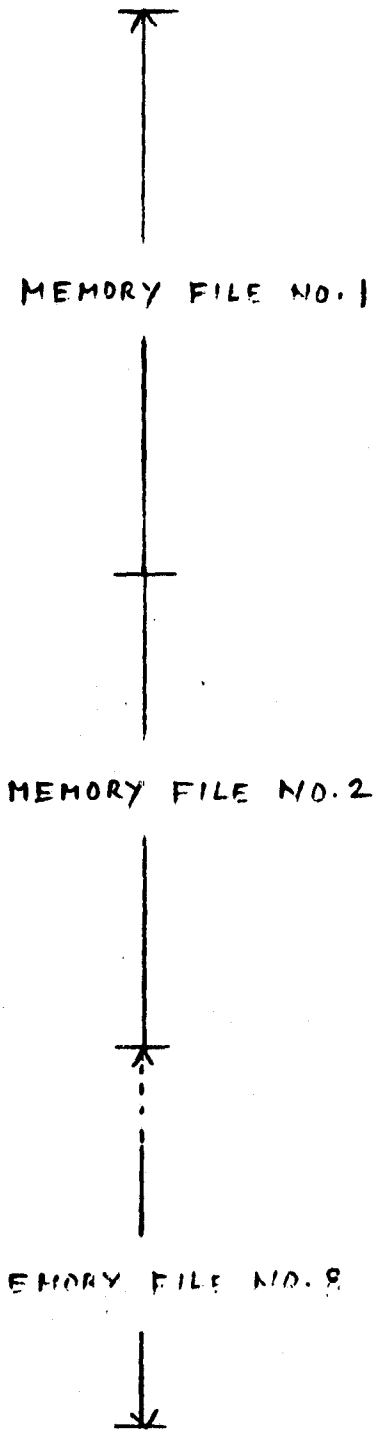
APPENDIX D

Impulsive 2-10 keV Solar Electron Events not Associated with Flares

IMPULSIVE 2–10 keV SOLAR ELECTRON EVENTS NOT ASSOCIATED WITH FLARES

DOUGLAS W. POTTER,[1] R. P. LIN, AND KINSEY A. ANDERSON[1]
Space Sciences Laboratory, University of California

ABSTRACT

Data from the *ISEE 3* satellite reveal a class of impulsive solar electron events with no measurable increase in flux above 10–20 keV. The flux histories and angular distributions indicate that the electrons propagate through interplanetary space with little or no scattering. The smooth extension of the power-law energy spectra down to the limit of the observations at 2 keV indicates that the electrons are accelerated at altitudes greater than $0.5\,R_\odot$ in the solar corona. Although these events occur more frequently than any other type of impulsive solar particle event observed, we have found no correlation with flares or flare-related activity. However, there is a close correlation with low-frequency (<1 MHz) type III radio bursts.

Our events are direct evidence for non–flare-associated, impulsive particle acceleration in the corona.

Subject headings: interplanetary medium — Sun: activity — Sun: corona — Sun: solar wind

I. INTRODUCTION

Energetic ions associated with solar flares were first detected in ionization chambers on the ground. Later, satellite measurements detected electrons and lower-energy ions. Nonrelativistic electrons were observed beginning in 1965 (Van Allen and Krimigis 1965; Anderson and Lin 1966). These impulsive solar particle events are usually associated with flares. Particle events limited to 10–100 keV electrons are often associated with minor flares or subflares (Lin 1974).

These observations extend to lower energies the range of observed solar particle emission. Although higher-energy events are associated with flares in the chromosphere, the smooth extension of the energy spectra down to the lower end of our energy range at 2 keV and the lack of association with the usual flare Hα emission and radio phenomena indicate that these low-energy events originate at high altitudes in the corona.

II. INSTRUMENTATION

The *ISEE 3* (*International Sun Earth Explorer*) spacecraft is ideally suited for making measurements of solar particles without interference from the Earth. Launched 1978 August 12, its unique orbit about the libration point on the Earth-Sun line (L_1, 230 Earth radii from the Earth) places it continuously in the interplanetary medium.

The University of California energetic particles experiment was designed to measure electrons from 2 to 1000 keV and ions from 50 keV to 40 MeV with high sensitivity (Fig. 1). The electrostatic analyzer consists of ∼10 cm diameter hemisphere plates separated by 0.75 cm and five funnel-mouthed spiral electron multipliers (spiraltrons) and was to measure electrons from 2 to 18 keV in 16 logarithmically spaced steps. A malfunction in the high-voltage supply has limited the

[1] Also Department of Physics.

upper energy to 8 keV. Two solid-state telescopes measure electrons above 16 keV and ions above 50 keV. All detector apertures have an opening angle of 15° in and ±25° normal to the ecliptic plane. Counts from each energy channel are divided into sixteen 22°.5 sectors in the ecliptic plane with respect to the magnetic field to provide angular distributions. A more complete description of the instrument is given by Anderson *et al.* (1978).

III. OBSERVATIONS

Figure 2 shows the flux histories of two characteristic examples of these low-energy impulsive solar electron events. The events show increases down to the lowest energy measured (1.9–2.1 keV). For the 1979 January 20 event, there is no increase in the lowest-energy channel (16–30 keV) of the telescopes. For the 1978 December 23 event, there is little or no increase in the 6.4 keV channel of the electrostatic analyzer. The relatively rapid rise and fall of the flux constitute the signature of a scatter-free event. The velocity dispersion is pronounced—the higher-energy particles arrive first.

Angular distributions taken during the peak of the 1979 January 20 event (Fig. 3) show that the electron fluxes are collimated in a narrow cone of full width at half-maximum less than one angular sector of 22°.5 that is directed away from the Sun along the magnetic field line. The extreme anisotropy and the rapid rise-rapid fall of the time profile indicate that the event is scatter-free.

To analyze the velocity dispersion, we assume that the particles were all released at the same time t_0 and traveled the same distance D from the source. Then

$$D = \beta c(t - t_0)$$

describes the relationship between onset time t and electron velocity βc. We determine the onset time for each energy channel by fitting a constant background
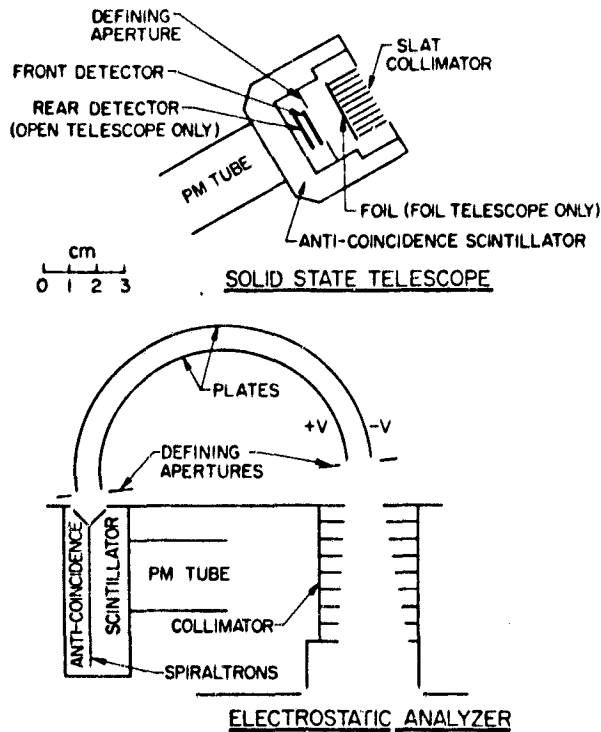
FIG. 1.—Schematic representation of the instrument

FIG. 2.—Electron flux on 1979 January 20 and 1978 December 23.

plus a linear ramp starting at the onset time to the time profile. A plot of the onset time versus inverse velocity for the 1979 January 20 event (Fig. 4) yields a straight line with slope equal to the path length and intercept equal to the release time. Accuracy of the calculated release time is usually better than ± 10 minutes. The path length of 1.3 AU is comparable to the length of a smooth spiral magnetic field line from the Sun to the Earth. We have analyzed more than 15 events in detail. All of them show relatively scatter-free time profiles and sharply peaked angular distributions. The calculated path lengths range from 1.1 to 1.5 AU. The path lengths from time dispersion analysis and the outward directed fluxes shown by the angular distributions demonstrate that these events are of solar origin.

To compute the energy spectra at injection, we subtract the relatively small sunward flux of returning particles and the pre-event background flux, and integrate over the duration of the event. A power law, $J \propto E^{-\gamma}$, where J is the differential particle flux and E is the particle energy, is generally a good fit to the spectra. As shown in Figure 5, the time-integrated spectra vary from event to event. The spectral exponent γ varies from 3.5 to 5. The spectra are often somewhat flatter at low energies.

These low-energy events occur frequently. In the 224 day period from 1978 October 31 to 1979 July 1, we have found ~100 impulsive solar particle events, ~50 of which are limited to less than 20 keV. The events tend to occur in clusters over several days; as many as six events have occurred in 1 day. The cluster-
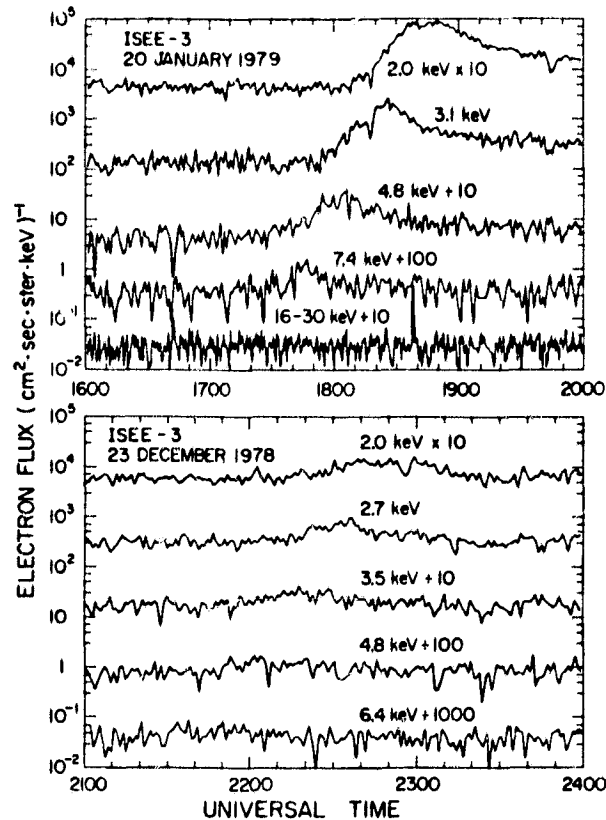
ing indicates that the events come from active regions and become observable as they pass across the portion of the solar disk where the magnetic field lines connect with the Earth.

We have searched for both radio bursts and Hα flares from ground-based observations as listed in the *Solar Geophysical Data* bulletins during the calculated release period for several events. Although we have not checked for events too faint to be reported, there is no correlation with listed events. We have compared some of our data with the University of California X-ray spectrometer on *ISEE 3* (Kane, private communication). No correlation with hard X-ray bursts was found. Although there were soft X-ray bursts during the calculated release period for some events, their occurrence appears to be random and due to the relatively large number of bursts. This lack of correlation with flare-related activity contrasts with higher-energy (10–100 keV) electron events which are closely associated with reported Hα flares and other flare-related phenomena.

Since low-energy electrons have a short range in the lower corona, the extension of the spectra to low energies implies that acceleration occurs high in the corona. To compute the acceleration altitude, we use a coronal density model derived from radio measurements (Fainberg and Stone, 1974) and Trubnikov's (1965) expression for the energy loss of electrons in a hydrogen

- 75 -

plasma. Starting with a power-law electron spectrum with $\gamma = 4$ at varying heights and assuming straight radially outward paths, we compute the resultant spectrum at Earth. Comparison with the observed spectra indicates that the electrons are accelerated at altitudes greater than $0.5\,R_\odot$.

We have also made a preliminary comparison with data from the Meudon/GSFC low-frequency radio instrument on *ISEE 3* for some events (Fainberg, Stone, and Steinberg, private communication). In every case, the arrival of the electrons coincides with an individual type III burst that is usually part of a low-frequency (<1 MHz) type III burst storm (Fainberg and Stone 1971, 1974).

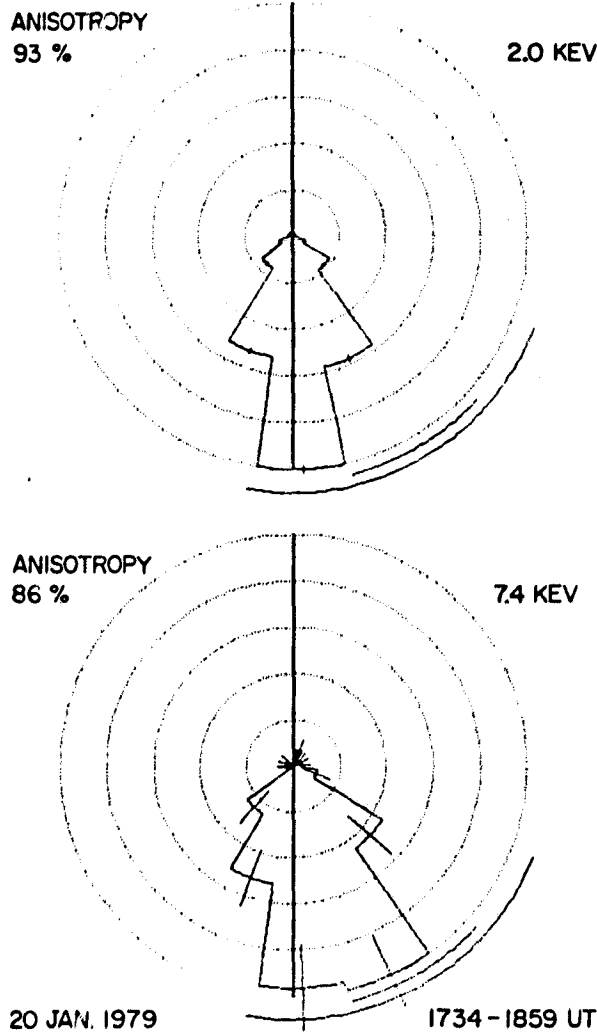FIG. 4.—Time dispersion analysis for 1979 January 20

FIG. 3.—Angular distributions taken during peak, 1979 January 20. The vertical line is the ecliptic component of the magnetic field. The outermost arc represents the limits and the next arc the average and standard deviation of the Sun position during the accumulation time. The (one-dimensional) anisotropy is calculated from $(f^+ - f^-)/(f^+ + f^-)$, where f^+ and f^- are the flux away from and toward the Sun, respectively.
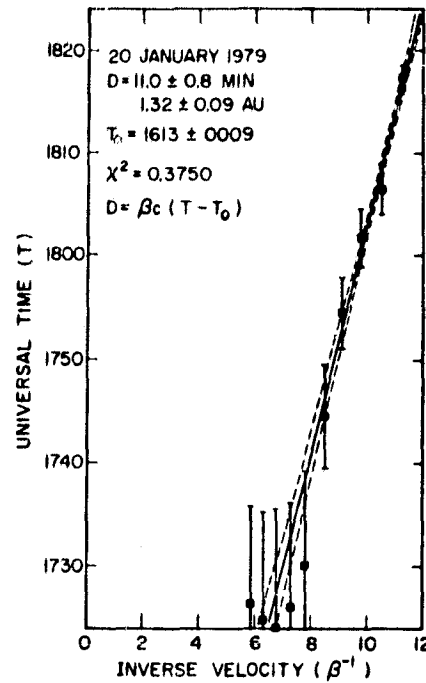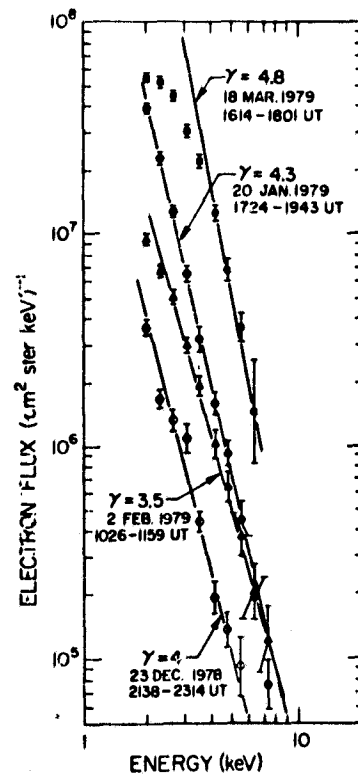

FIG. 5.—Time-integrated energy spectra of events on 1979 January 20, 1978 December 23, 1979 February 2, and 1979 March 18. γ is the spectral exponent.

IV. DISCUSSION

If we assume that the electrons are emitted in a cone the width of an active region ($\sim 60°$), the total energy released in one of these events is on the order of 10^{25} ergs. If the magnetic field in the acceleration region is about 1 gauss, the acceleration could be produced by conversion of magnetic to kinetic energy over a volume having linear dimension on the order of $10^{-2}\ R_\odot$. Thus the energy requirement for these particle events is easily met despite the high altitude.

REFERENCES

Anderson, K. A., and Lin, R. P. 1966, *Phys. Rev. Letters*, **16**, 1121.
Anderson, K. A., Lin, R. P., Potter, D. W., and Heetderks, H. D. 1978, *IEEE Trans. Geosci. Elect.*, **GE-16**, 153.
Fainberg, J., and Stone, R. G. 1971, *Solar Phys.*, **17**, 392.
———. 1974, *Space Sci. Rev.*, **16**, 145.

Lin, R. P. 1974, *Space Sci. Rev.*, **16**, 189.
Trubnikov, B. A. 1965, *Rev. Plasma Phys.*, **1**, 105.
Van Allen, J. A., and Krimigis, S. M. 1965, *J. Geophys. Res.*, **70**, 5737.

KINSEY A. ANDERSON, R. P. LIN, and DOUGLAS W. POTTER: Space Sciences Laboratory University of California, Berkeley, CA 94720